uc3m | Universidad Carlos III de Madrid

University Degree in Energy Engineering
Academic Year (2018-2019)

Bachelor Thesis

"Development of a cellular automata consistent with enhanced-regime-transport in tokamaks for fusion applications"

Daniel Medina Roque

Tutor

Luis Raúl Sánchez Fernández

July 2019. EPS Leganés, Madrid.

ABSTRACT

Nuclear fusion has huge expectations of becoming a revolutionary energy source in the short-term future. The upcoming increase of electricity demand in developed countries, together with fusion environmental, safety and economic benefits make it a more than reliable alternative to the existing energy sources.

The big difficulty of fusion during the more than 50 years of research has always been the demonstration of its reliability. Two main different approaches have been the most promising ones: The Inertial Confinement Fusion (ICF) aiming to high plasma densities by its compression with powerful lasers and the Magnetic Confinement Fusion (MCF) aiming at low densities by the use of magnetic fields, with two main differentiated designs: stellarators and tokamaks.

Tokamaks research has defined them as the best alternative to make "fusion electricity" a reality. In this context, ITER, the most revolutionary experiment of human history, is currently being built in Cadarache (France) to prove fusion feasibility, achieving a positive net energy balance. If successful it will be continued by DEMO, which would be the first grid-connected nuclear fusion power plant.

Temperature inside tokamaks is of the order of 100-150 million K at which matter is only found in plasma state, the forth state of matter. Fusion plasmas are known to be turbulent, the high gradients they are subjected to induce severe instabilities that make their confinement a true challenge. As a consequence of these instabilities plasma escapes from the confinement volume, diminishing the efficiency of the reaction and causing catastrophic damage of the reactor components. A reliable magnetic confinement is critical for the feasibility of the tokamak design.

To this matter, various confinement regimes are found in tokamaks when the external power is increased. Starting from the "ohmic heating", then the L-mode (Low confinement mode) and finally reaching the H-mode (High confinement mode), being this last one the most promising one to be used in industrial fusion process. But still, there are too many unknowns to the dynamic processes governing this regime.

In H-mode, the strong turbulence at the outer layers induce a significant poloidal plasma rotation causing the appearance of the so-called edge transport barrier (ETB) that reduces the radial particle drift, improving the confinement. Nowadays, the transport dynamics of this regimes are still not fully understood, transport in L-mode is proved to be non-diffusive and similar to "SOC dynamics" (SOC =Self Organized Criticality), while H-mode is characterized by a reduction of the memory and the appearance of a sheared flow when compared with the L-mode dynamics.

As a starting point to understand the relation between turbulence and shear in the H-mode, the present project focuses in the creation of a model that recreates the basic dynamics of the turbulent transport inside tokamaks. The developed model needs to have a realistic behavior, allowing the detection of the fundamental relations and the essential variations of the dynamic variables for further investigation.

To achieve this goal, a model aimed to capture the basic dynamics of the H-mode plasma, introduced in 2018 by the Aerospace student in the university Carlos III of Madrid Cristina Midori Fukuda León, is modified to resemble two main processes that the original model failed to achieve:

- The randomization of the transport phenomena, since the shear affects the turbulence eddies responsible of the transport reducing their size and lifetime, causing some particles to remain in their current magnetic surface instead of jumping to an external one. This is introduced by the transport probability variable "Pk" that reduces the transport when shear values are increased.

- The reduction of the long-term memory of the system, since shear reduces the influence of previous avalanches in the occurrence of avalanches at the present time. This is done by making the gradient profile to be locally supercritical, with avalanches occurring at every iteration, regardless of their historic values.

The second modification is demonstrated to work properly by the Hurst Rescaled Range method to detect memory in stationary time series, which provides evidence that the process approaches the behavior of a random walk when the profile is supercritical.

The conclusion of this project is the quantification of the effect of the new introduced variables and relations. The transfer entropy analysis tool is used to study the causality between the most important variables to be able to predict the induced one by knowing the values of the dominant variable in a real tokamak.

As future research more realistic ways of implanting the turbulence-shear interactions could be introduced when discovered and could also help to bring fusion energy research closer to people, helping them to better understand the physical underlying processes and to become less unwilling to fusion when informed about the enormous advantages and potential of fusion over the rest of energy sources.

Keywords: Nuclear Fusion, Energy, Tokamak, H-Mode, Sandpile, Confinement, SOC, Transfer Entropy, Hurst Rescaled Range, Shear and Turbulence.

ACKNOWLEDGEMENTS

To prof. Luis Raúl Sánchez Fernández for your guidance during every step of this project, your good will, your availability at any moment and the time you have devoted. Thank you for teaching me all these very interesting things about fusion energy that I was very interested but didn't know before. I will always remember your comment "This is how science works" when things do not work as expected at any aspect of my life, making me look from another point of view and finding an alternative solution. Your kindness, your investigative curiosity and your patience makes you an example to me. When I asked my professor from Nuclear Energy to do the thesis in this field and she gave your contact, I could never imagine this trip being this meaningful and amazing. You have introduced me to the fascinating world of fusion energy and I do not see myself abandoning it in the rest of my life.

To Cristina Midori Fukuda León for your interest and your selfless help at any moment of the development of this project. Your previous work in this field was the inspiration and guidance I needed for the fulfillment of my objectives. Thank you.

To some students of the European Master of Science in Nuclear Fusion and Engineering Physics whose unconditional advice and cooperative spirit have make me even more interested and amazed about the beautiful fusion scientific community.

To my family for supporting me, for pushing their selves to understand what I was doing and for being such a source of happiness and release in the hard times.

Lastly, to all my friends and to anybody that knows what fusion means to me, I am very pleased for sharing this phase of my life with you. There is no better definition of love than your feedback when I share my interests and achievements. I love you all.

CONTENTS

LIST OF FIGURES

LIST OF TABLES

1. INTRODUCTION TO NUCLEAR FUSION

1.1 Nuclear fusion physics and reaction

Nuclear Fusion has been powering the stars for thousands of millions years, but was first discovered by Arthur Eddington in 1920. This concept is explained as a thermonuclear process that takes place when light nuclei fuse together and become a heavier nucleus while realizing huge amounts of energy [1].

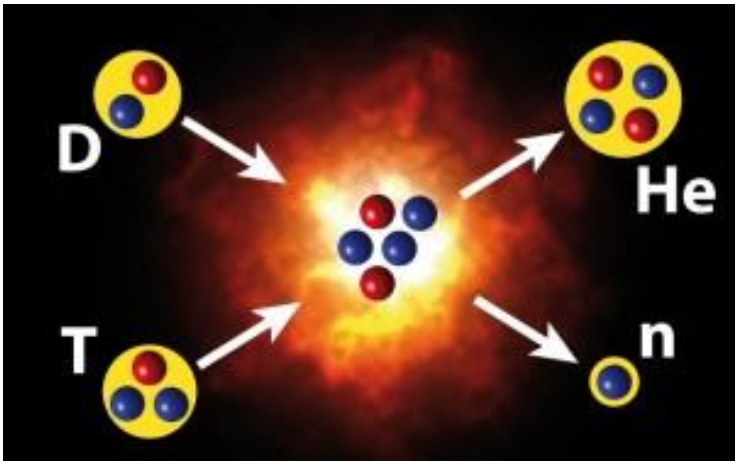

Figure 1.1 Deuterium-Tritium fusion reaction [Credits to: National Fusion Laboratory CIEMAT http://www.fusion.ciemat.es/]

Energy is produced by the difference in mass between fusion reactants and products and calculated with Einstein´s famous formula [2]:

$$E = \Delta m c^2 \tag{1.1}$$

There is a mass defect, since the mass of the separated subatomic particles is greater than the mass of the nucleus that they form together, and that missing mass is transformed into energy.

For fusion to take place, nuclei have to come extremely close, since they are positively charged and repel each other at large distances ($d \gg 10^{-15}$), but they are mutually attracted instead, if they hold sufficient relative kinetic energy to overcome the electrostatic barrier and enter the range where nuclear strong forces are dominant ($d \sim 10^{-15}$). In other words, they have to collide at sufficient velocity to surpass their mutual repulsion [3].

The velocity of the particles and the relative kinetic energy between them is immensely affected by temperature, which in the centre of the Sun is around $10^7 K$. At this range of

temperatures matter is in a **plasma state**, the forth state of matter, defined as *an ionized gas formed by free electrons and positively charged nuclei, in such proportions so that there is no net electric charge, and that interact with each other by means of electric and magnetic fields.*

Achieving this range of temperatures in a controlled environment on Earth has been a challenge for the scientific nuclear community. Specially knowing that the Sun, due to its massive size, could operate far from its most efficient temperature due to the low limitations of fuel mass and volume, but for electricity production, the best possible efficiency is mandatory and leads to even higher temperatures in experimental reactors around 100-150 million K.

1.2 Fusion fuel

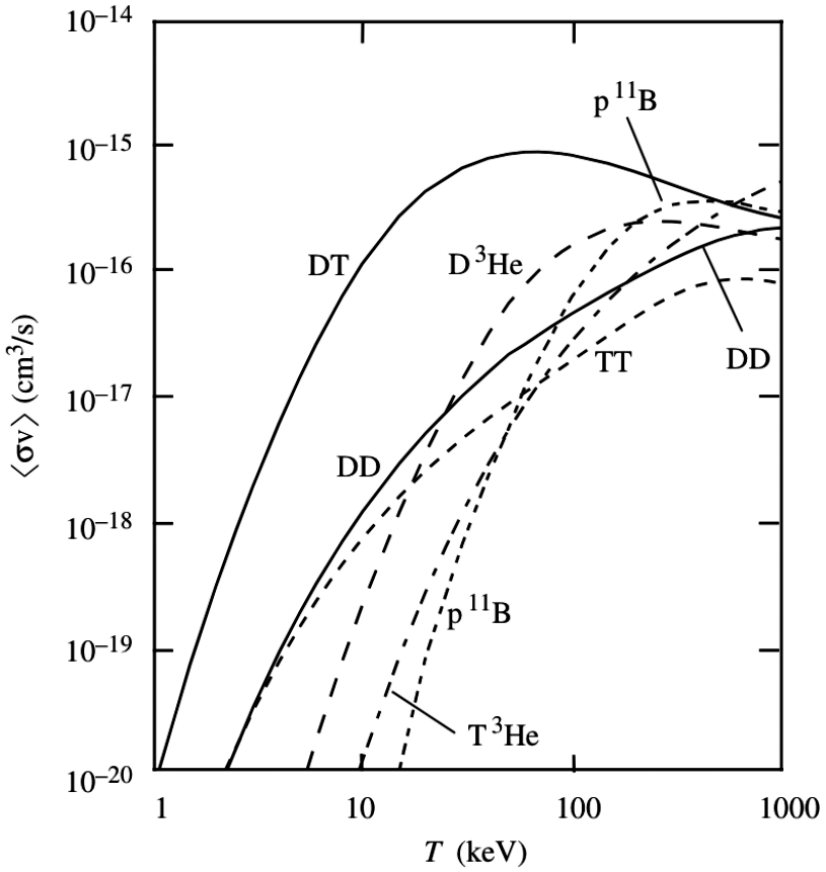

Figure 1.2 Reactivity as a function of temperature for several studied fuels [Credits to Ref [4]]

Among other candidates for fusion reactions and searching for maximum efficiency, the pair Deuterium-Tritium has been identified as the best choice since it presents a peak for maximum reactivity (and maximum energy realised) at the lowest temperatures, within the range 50 – 100 million degrees [4].

The Coulomb barrier is easier to overcome for hydrogen isotopes since their nuclei contain only one proton and their mutual repulsion is lower than in the case of heavier elements.

Deuterium is a harmless and widely available resource that can be distilled from seawater at $33g/m^3$. Tritium is a fast-decaying radioelement of hydrogen that must be produced. In future reactors, it will be mainly produced inside the fusion reactor when neutrons escaping the plasma are absorbed by the lithium in the blanket wall of the tokamak, this process is commonly called "**tritium breeding**".

This process has a huge potential since it could allow tritium self-sustainment in the reactor by the introduction of lithium, which is also an abundant and easily extracted material from superficial layers of the Earth and almost unlimited when extracted from seawater. In current experiments, however, tritium must be produced outside of the reactor by other means, typically by bombarding lithium with neutrons in an accelerator.

1.3 The triple product

Assuming equal proportions of deuterium and tritium, the performance of a fusion reactor candidate can be characterized in terms of the so-called "*The triple product $nT\tau$",* where n stands for density, T for temperature and τ for confinement time.

In order to assure the reactor's feasibility, **breakeven** (Q>1) must be achieved. Breakeven is the state at which the energy produced by nuclear fusion exceeds the energy losses, to be reached John Lawson`s criteria (1950s) must be fulfilled [5]:

$$n \times T \times \tau \geq 3\ x10^{21} \qquad [KeV \cdot s \cdot m^{-3}] \tag{1.2}$$

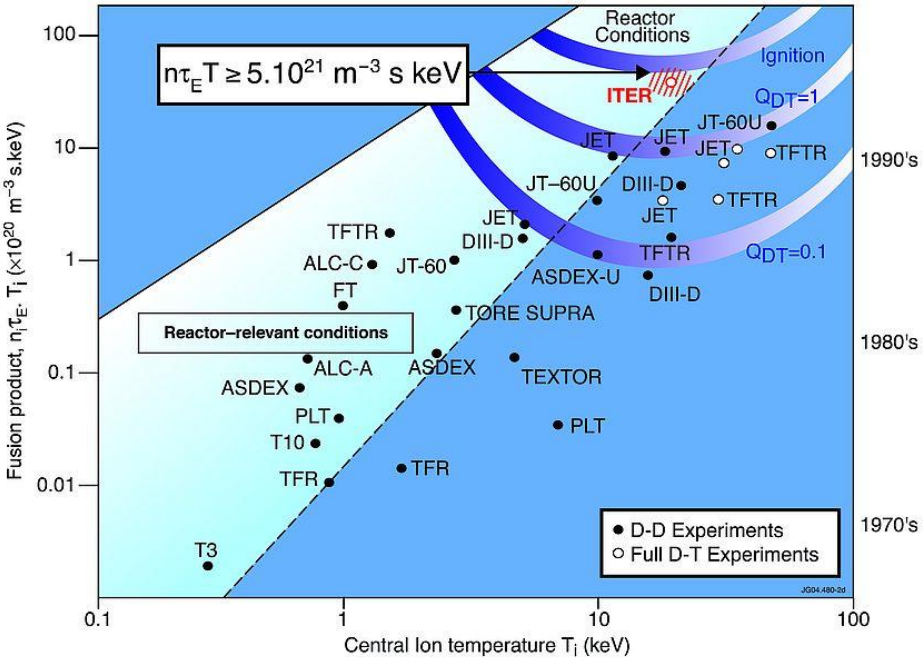

Figure 1.3 Progress in the fulfillment of John Lawson`s criteria by the different experiments [Credits to: Eurofusion www.euro-fusion.org]

The temperature has already been prescribed to achieve the highest efficiency with the lowest temperature. Then to reach breakeven, the other two terms, confinement time and density, must be adjusted, leading to two types of fusion reactor approaches: Inertial Confinement Fusion (**ICF)** and Magnetic Confinement Fusion (**MCF).**

1.4 Fusion reactors

Several approaches to surpassing Lawson's criteria have been attempted over the years. The two most successful ones to date are inertial and magnetic confinement fusion.

1.4.1 Inertial confinement fusion (ICF)

In ICF, the plasma is compressed by means of powerful lasers aiming at reaching very large densities, $n \sim (10^{30} - 10^{31})m^{-3}$ although for very short confinement times, $\tau \sim (10^{-10} - 10^{-9})s$.

The most important facility in the context of ICF is the NIF (National Ignition Facility) which uses the **indirect drive method** in which the DT fuel capsule is located inside a gold or depleted uranium hohlraum, which is a cylindrical recipient with open ends. The 192-beam and 2.15 MJ laser strikes the hohlraum creating a rain of x rays that causes the capsule to implode, extremely heating and compressing the DT fuel into a hot spot. Fusion reaction is started producing an alpha particle and a neutron, but for ignition to

take place sufficient alpha particles must be present to generate the heat needed to initiate a chain of further fusion reactions within the hotspot [6].

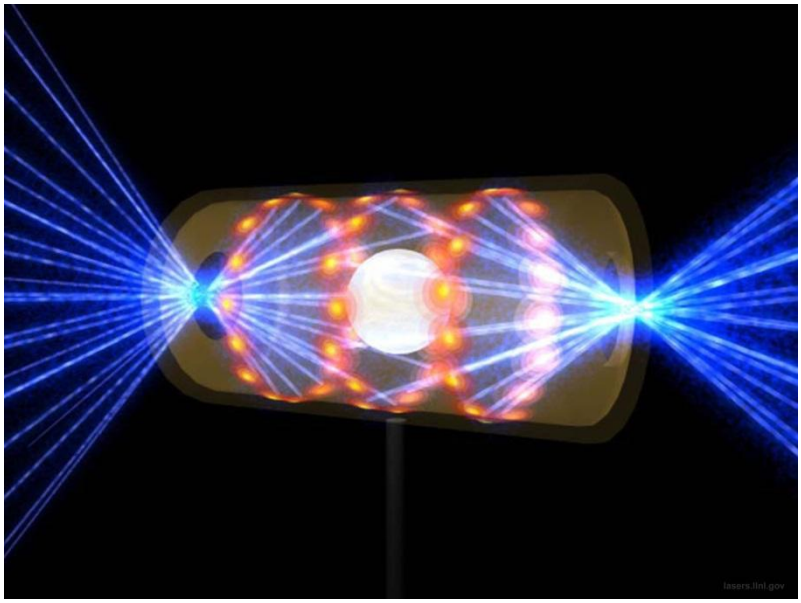

Figure 1.4 Indirect drive method of ICF [Credits to: National Ignition Facility https://lasers.llnl.gov/]

Research groups and laboratories in Inertial Confinement are still investigating ways of achieving breakeven (Q>1) by increasing the symmetry and uniformity in the distribution of the DT capsule compression, which will lead to significantly higher produced energy. However, the rate at which DT capsules will have to be introduced in the reactor in order to reach feasibility in electrical production would be of the order of 10 pellets per second and now they are working with one every few hours.

ICF facilities have also been strongly supported from other areas outside of fusion energy, since they can be used to support nuclear weapon development and to investigate space plasmas and planet formation physics. This is in contrast to magnetic confinement fusion, whose focus is solely and foremost on electricity production.

1.4.2 Magnetic confinement fusion (MCF):

In MCF, the plasma is confined by means of magnetic fields aiming at achieving moderate densities, $n \sim (10^{20} - 10^{21})\, m^{-3}$ but for much longer confinement times, $\tau \sim (1 - 10)\, s$.

The elemental principle underlying this approach is the fact that all plasma constituents have a net electric charge, being positive for ions and negative for electrons, and will describe helical trajectories around the lines of the magnetic field as a result of the action of Lorenz forces. In order to find a proper magnetic configuration, the plasma can be kept inside a confined volume where plasma particles can freely move along the

magnetic field lines while being accumulated and heated, achieving the conditions needed for fusion at sufficient distance from the reactor walls to prevent material damage [7].

In order to achieve that configuration, the easiest theoretical design would be a toroidal disposition of magnetic coils to induce a purely toroidal magnetic field lines that close themselves at the end of each turn. Maxwell equations however force a magnetic field gradient to appear in the radial direction that ultimately induces a radial particle drift that pushes the plasma out of the confining volume.

An additional poloidal component of the magnetic field lines on top of the toroidal one previously mentioned is needed to avoid the particle drift. The way of inducing this poloidal component differentiates the two main MCF toroidal configurations: stellarators and tokamaks.

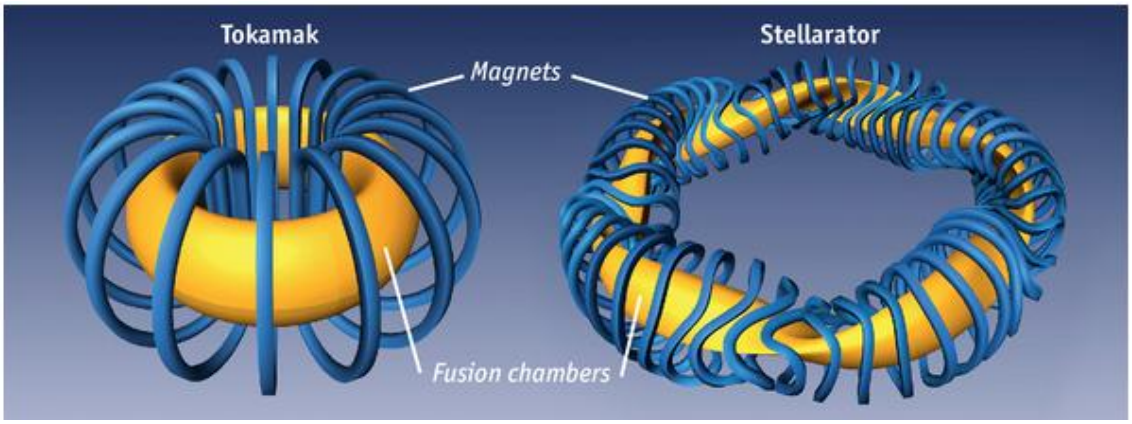

Figure 1.5 Structural comparison between tokamak and stellarator configurations. [Credits to: International Atomic Energy Agency www.iaea.org]

- Stellarators:

In stellarators the poloidal component of the magnetic field is created by means of another set of external magnetic coils, in the same that is done for the toroidal one.

In stellarators, the toroidal plasma current is very small, even negligible when high structural optimization is realized. An important property of stellarators is the fact that they can be operated **steadily** and can avoid Magnetohydrodynamic (MHD) instabilities such as disruptions. These characteristics might suggest an advantage over tokamaks, making stellarators the most theoretically feasible configuration for a future fusion reactor [8].

However, the main drawback of this configuration is that the plasma is no longer toroidally symmetric, which highly increases collisional diffusive losses and causes topologies as **magnetic islands** and **stochastic regions**, decreasing the constraints of particle motion and therefore harming the confinement properties and making stellarators rather worse than tokamaks working with similar parameters.

However, there have been several improvements in the last decades, achieving *quasi-symmetries* through new designs adapted to the requirements and based on heavy numerical optimizations. The main experiment currently in operation is the Wendelstein 7-X in Greifswald (Germany), which proposes an alternative configuration to the tokamak, achieving symmetries through extremely complicated designs and could set the basis for a new generation of devices that solves the actual concerns of the tokamak configuration and finally makes fusion a feasible source of energy.

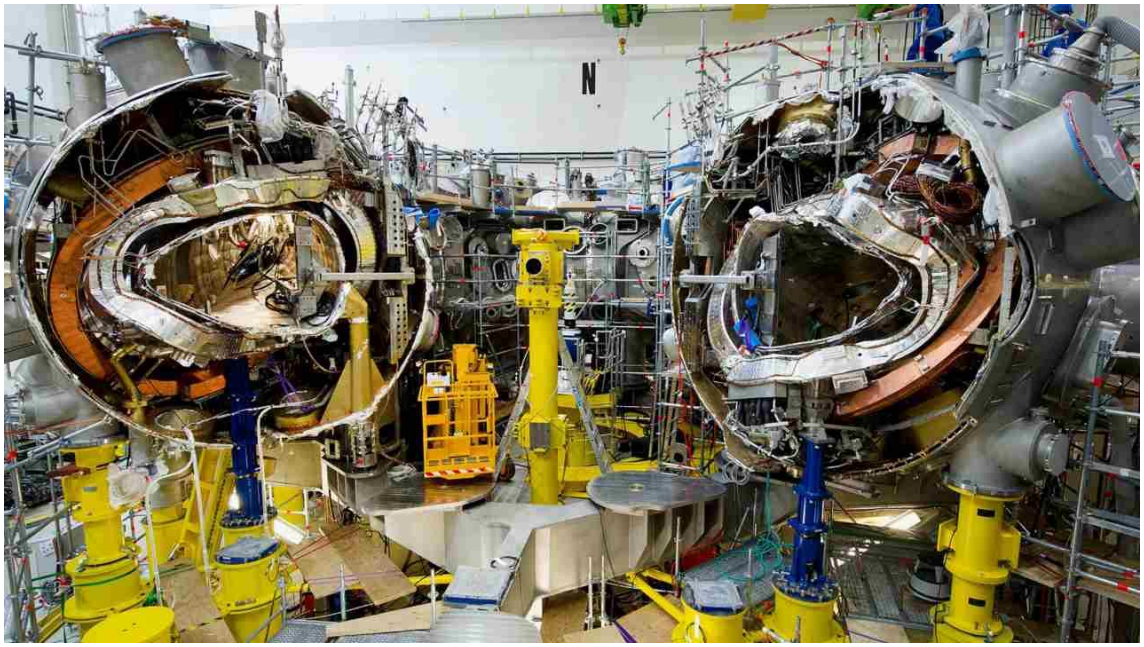

Figure 1.6 Wendelstein 7-X complicated designs construction [Credits to Max-Planck-Gesellschaft www.mpg.de/]

- Tokamaks:

Tokamaks generate the poloidal component by driving a huge toroidal current, of the order of several millions of Amperes, through the confined and highly conductive plasma. The created poloidal magnetic field is sufficient to generate the required twist of the magnetic field lines, but is still significantly lower than the toroidal component.

The plasma current is induced by a transformer effect (in which plasma acts as the secondary) that is impossible to sustain in steady state and forces the tokamak configuration to be **intrinsically pulsed** (although alternative ways to drive current are being explored that might bring the tokamak closer to steady-state operation in the future) [9]. This might have some implication on the management of the supply to the electric grid and the fatigue of the components when working as a power plant.

The confined plasma is toroidally symmetric, which reduces the appearance of magnetic islands and stochastic volumes and therefore restricts the possible motions of the confined particles enhancing its confinement properties significantly over the stellarators.

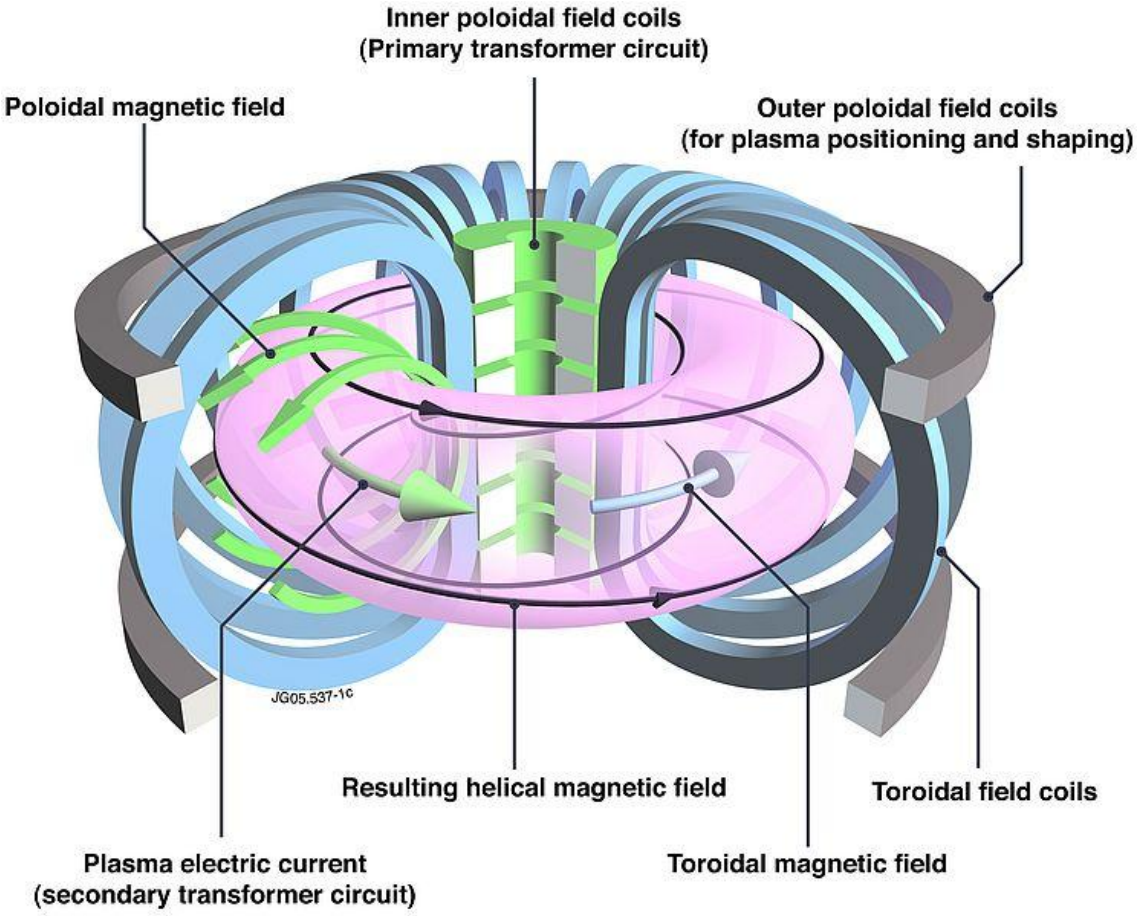

Figure 1.7 Illustration of the tokamak magnetic principle: configuration of magnetic coils resulting in confining magnetic fields [Credits to EUROfusion: www.euro-fusion.org]

But the extremely large current flowing in the toroidal direction of the tokamak offers a big source of free energy for the development of instabilities, especially **disruptions**, which must be monitored and controlled. Otherwise, uncontrolled disruptions may cause a large fraction of the stored plasma energy to be ejected towards the reactor walls in a very short period of time causing critical and irreparable damage. During disruptions, very strong electromagnetic forces are generated and a significant number of **runaway electrons** [10] can be created, which could reach energies of tens of MeV and also damage the main components of the reactor.

TABLE 1.1. COMPARISON BETWEEN STELLARATOR AND TOKAMAK MAIN CHARACTERISTICS

Characteristic	Stellarator	Tokamak
Toroidal symmetry ↓ Magnetic islands Stochastic regions	Low Very important	Very high Negligible
Generation of poloidal component Operation	External magnetic coils ↓ Continuous and steady	Induced toroidal current ↓ Pulsed
Toroidal current ↓ Disruptions Electron runaway	Negligible Negligible	Enormous Very important

Table 1.1 shows the different implemented methods showing in green the beneficial features and in red the counter-productive effects of the technology. Both are in theory very similar for both configurations, but experimentally tokamaks have been demonstrated to be the most promising design and have expectations to make grid-connected fusion power plants a reality in the following years.

The flagship of MCF is the ITER (International Thermonuclear Experimental Reactor) tokamak experiment, the most ambitious energy project in the human history. It will be the largest tokamak on Earth and will start its operation in the early 2020s. If successful, it will be the first machine able to reach breakeven and even confine an ignited plasma. Its goal is to prove the feasibility of nuclear fusion via the MCF approach by the completion of its 5 goals:

1. Produce 500 MW of fusion power at pulses of 400s from less than 50MW of injected heating power, achieving Q>10.

2. Demonstrate the technological needs for future fusion plants, since it is ten times bigger than JET, the largest machine operating today, and scientist will be able to test technologies at real scale.

3. Achieve **internal heating**, because in burning plasma the energy of the produced helium nuclei exceeds the one injected by external sources and could be used to heat the plasma and sustain the reaction.

4. Test **tritium breeding**, producing the needed tritium within the reactor through the absorption of neutrons by the lithium in the tokamak blanket and use it as fuel for further reactions.

5. Prove the safety characteristics of fusion devices, specially the easy stop of the reactor in case of emergency and the negligible pollution of the environment during its operation.

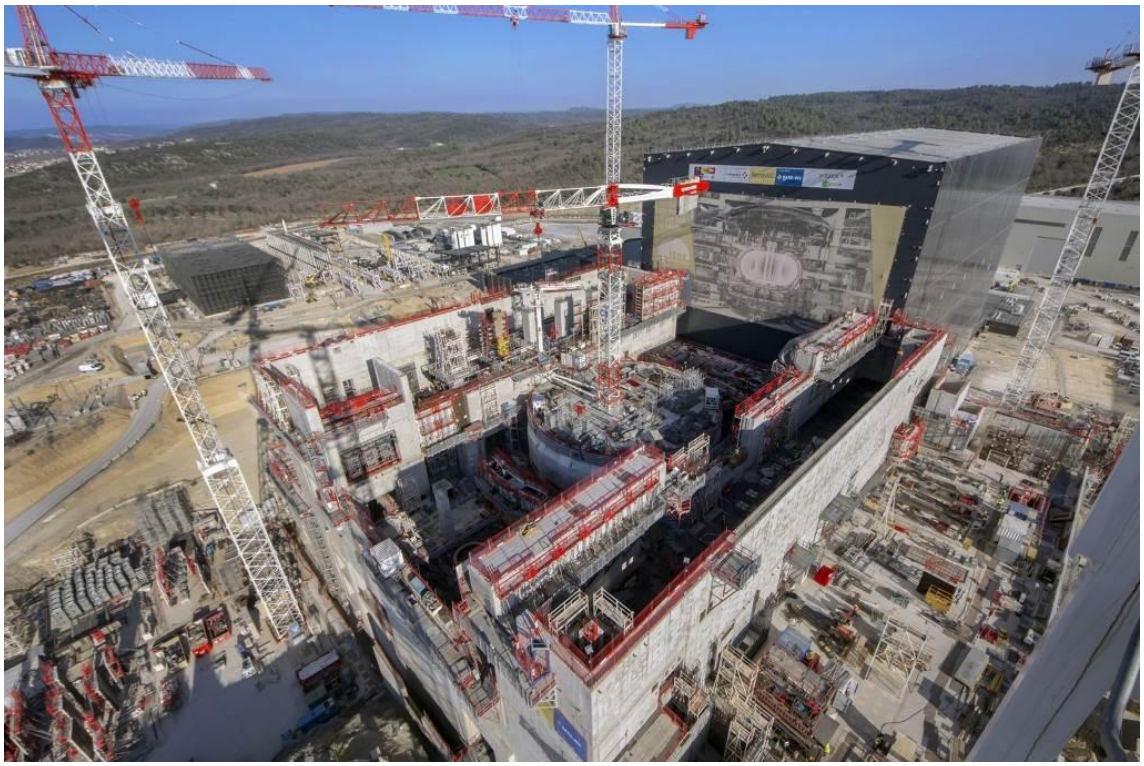

Figure 1.8 Construction of ITER tokamak in Cadarache (France), March 2019 [Credits to ITER organization www.iter.org]

2. TOKAMAK TRANSPORT PHENOMENA AND CELLULAR AUTOMATA

2.1 Transport in tokamaks

In tokamaks, magnetically confined plasmas are subjected to large radial gradients (of density, pressure and temperature) that make them strongly unstable and turbulent. These strong gradients are forced to keep the plasma within the confined volume sufficient time to fulfil the John Lawson`s criteria. At the same time they also drive strong electrostatic potential fluctuations that lead to vortex structures called **turbulent eddies**, aligned with the local magnetic field, that enhance the particle radial drifts. As a result, the energy and density of the plasma decreases, therefore deteriorating the needed conditions and making fusion even harder to achieve.

In this regard it is of extreme importance to understand the particle and energy transport in tokamaks in order to be able to ease the start of the reaction. Different confinement regimes were experimentally discovered in tokamaks as the external heating that drives them is increased. Since a good knowledge of the characteristics of these regimes is the basis of all further studies in this project, we discuss them briefly in what follows.

2.2 Confinement regimes

As the external heating power is increased, the turbulent phenomena in the plasma and the particle drifts out of the toroidal volume change importantly. Leading to different confinement regimes whose characteristic radial pressure gradients are outlined in the following figure [3].

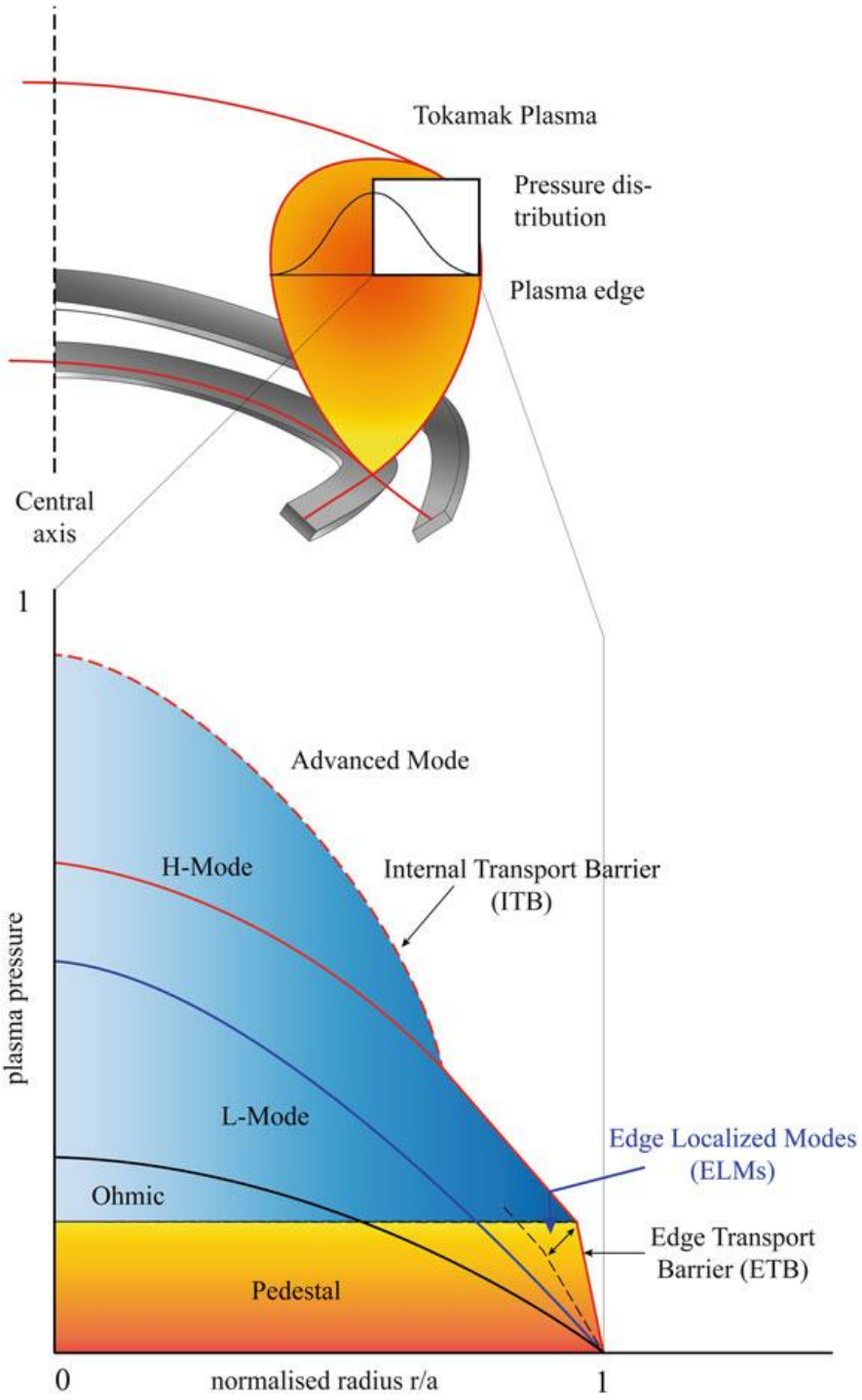

Figure 2.9 Radial pressure profiles for the main tokamak confinement regimes: ohmic (black), L-mode (blue), H-mode (red, solid) and advanced modes (red, dashed)

The plasma starts to be heated in the "**Ohmic heating**" region, where the large toroidal current across the plasma heats the plasma via Joule effect. However, since the plasma electrical resistivity diminishes as temperature increases ($\eta \sim T^{-3/2}$), additional external heating is soon needed that must be provided via wave or neutral beams heating. The radial profiles of the plasma become more and more steeper as they are heated more strongly until reaching a point, where the tokamak confinement behaviour changes abruptly and the profile suddenly stops responding to heating power variations

and remains clamped. This state is called the **L-mode**. In this regime, very interesting and surprising dynamics take place. First, the plasma profiles seem to be insensitive to the location and strength of the drive, which runs counter intuitively to what one might expect in a diffusive system. In addition, perturbations of the profiles can propagate ballistically in the radial direction, again in contrast to usual diffusive behaviour [11]. Avalanching behaviour in the radial direction and out of the plasma is also observed.

At even higher external power, above a certain threshold a "pedestal" and new features appear. In particular, the bottom of the radial pressure and temperature profiles rise, increasing its steepness. Within this pedestal region, the plasma seems to be rotating in the poloidal direction with a speed that varies with the radial position. This type of rotation is called a sheared flow. Radial transport through this pedestal is strongly reduced, which explains the formation of the steeper pedestal [12]. When the pedestal arises it is said that the plasma transitions into the so called **H-mode**, characterized by the presence of the **edge transport barrier** (ETB) [13]. The characteristics of transport in H-mode are quite different from the L-mode, particularly over the barrier region, where more-diffusive-like features are recovered.

Finally, it is also worth mentioning that additional advanced confinement regimes have been reached by the excitation of **internal transport barriers** (ITBs), which are inner plasma radial regions of reduced transport.

2.3 Cellular Automata representation of the L-mode

The dynamics of radial transport in tokamaks have been investigated in L-mode by using a cellular automata approach that captures its basic features.

2.3.1 Transport mechanism in L-mode

In the L-mode the stiff radial gradients of pressure and temperature are invariant to variations in the heating source. This stiffness has been associated by some authors to the relevance for turbulent transport of near marginal conditions, similar to what are known to lead to the **self-organized critical (SOC) state** [14]. As a result, the radial transport in this near marginal conditions obeys non-diffusive transport laws and exhibits features such as self-similarity and memory. A very intuitive and useful tool used to capture the basis of the L-mode transport mechanism is a cellular automata: the running sandpile model [15].

2.3.2 The running sandpile model

The running sandpile is a two dimensional cellular automata, where there are N cells storing grains of sand. Each iteration starts with a continuous and random rain of sand grains over the sandpile, having each sandpile cell a prescribed probability "P_o" of receiving a prescribed number of grains "N_b" in each iteration. The grains are stored in

the cell they have fallen in, therefore increasing the height of the cell, until the difference in heights of the corresponding cell and the one to its right exceeds a prescribed critical threshold value "Z_c". At this moment the cell becomes unstable and transfers a prescribed number of grains "N_f" to the cell to the right. When the rightmost cell of the system becomes unstable, "N_f" grains are expelled as a mass outflow of the sandpile. This functioning is graphically described in figure 2.2.

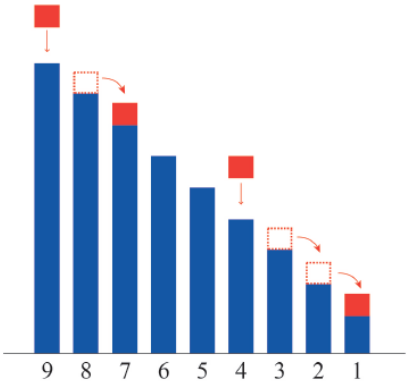

Figure 2.10 Functioning scheme of running sandpile

It is important to remark the fact that the transfer of "N_f" grains from one cell to the next one can cause the second one to be unstable in the following iteration. This causes what is called **avalanche**, explained as continuous transport of "N_f" grains between pairs of adjacent cells during consecutive iterations. Because the fact of the first cell being unstable and dropping grains onto the second, can cause it to become unstable and to transport the grains to a third one. Moreover, the transport of the first cell can also make the cell to its left to become unstable, starting two avalanches at the same time. Both cases are illustrated in figure 2.3.

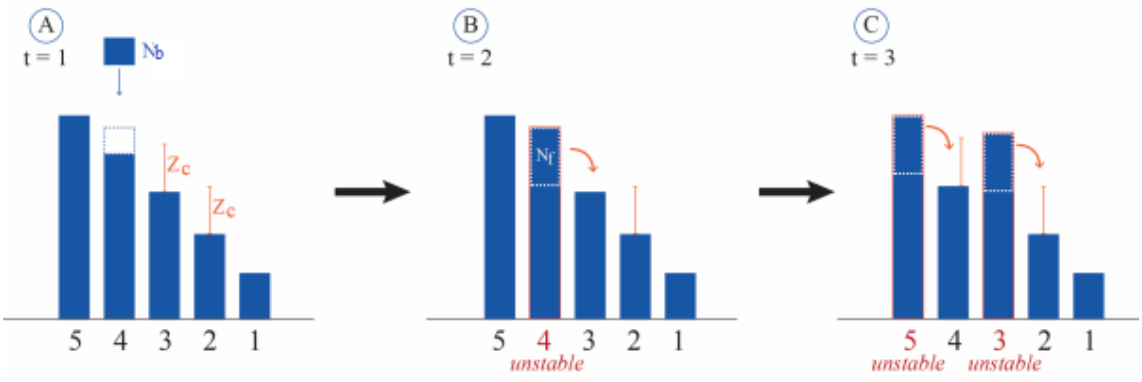

Figure 2.11 Avalanche mechanism in sandpile model

After a sufficiently large amount of iterations, the sandpile eventually reaches by itself a stationary state where the sand losses at the rightmost cell balance the mass income due to the rain over the system. This is the so called SOC state and is characterized by local

gradient constantly close to critical values and transport only produced by means of avalanches, causing confining times demonstrated to be lower than in the diffusive transport [16] .

2.3.3 Sandpile variables and their relation to tokamak physics

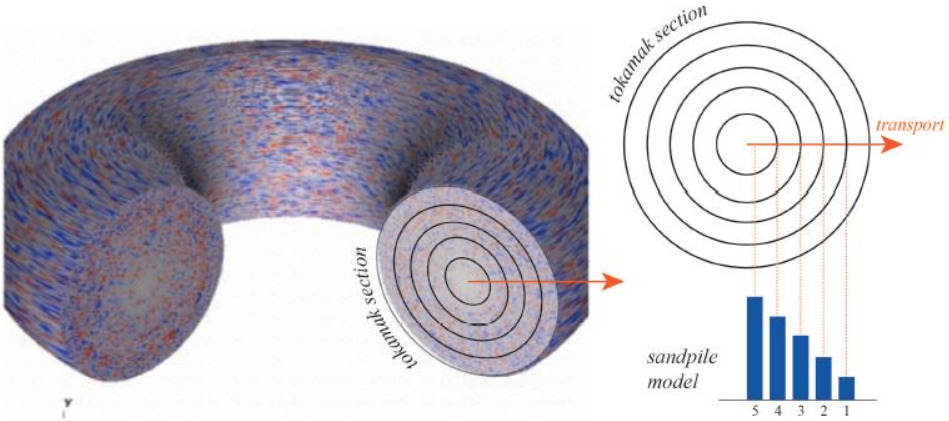

Figure 2.12 Relation between tokamak and sandpile model transport mechanisms.

In the CA representation of the L-mode, each cell represents a different rational magnetic surface in the radial direction, where the most important instabilities are located. The random rain increasing the height of the cells plays the role of the external drive of the tokamak, heating the plasma from the centre of the confined volume and increasing the profiles of all relevant plasma physical properties.

The critical threshold which induces the transport of "N_f" grains between adjacent cells, represents any critical pressure or temperature gradient that, when locally surpassed, generates turbulence, that itself leads to increased plasma radial transport until the local profile is relaxed below the critical threshold.

TABLE 2.1 REAL MEANING OF SANDPILE VARIABLES

Variable	Sandpile meaning	Real tokamak meaning
N	Amount of cells	Amount of magnetic surfaces (MS)
h_n	Sang height of each cell	Local pressure or energy of each MS
N_b	Number of fallen grains	External drive strength
Z_c	Critical gradient	Local threshold of instability
N_f	Grains transported by unstable cell	Transport of particles between MSs

2.3.4 Rules and steps of the cellular automata that mimics the L-mode tokamak

1. Sand rain

The cells receiving N_b are decided according to Rule 1.

Rule 1: There is a probability of P_o for each cell to receive N_b grains

2. Unstable cells search.

2.1 Calculate the height gradient "Z_n" in each cell n according to:

$$Z_n = h_n - h_{n+1} \tag{2.1}$$

2.2 Check if any local gradient Z_n exceed the critical threshold, according to rule 2, in that case define that cell as unstable.

Rule 2: A cell n is unstable if $Z_n > Z_c$

3. System relaxation when unstable.

Transfer the number of grains set by rule 3.

Rule 3: Each unstable cell will transfer N_f grains to the one to its right.

2.4 Cellular Automata representation of the H-mode

2.4.1 Transport mechanism in H-mode

When the plasma is heated above a certain power threshold, its profile is suddenly self-rearranged and it reaches the H-mode.

The H in H-mode comes from "High confinement". It is a strong unexpected change in plasma characteristics whose origin is still not fully understood. While the inner radial part of the plasma behaves basically in the same way as in L-mode, the strong turbulence at the external layers drive a strong poloidal plasma rotation, causing the appearance of the so-called Edge Transport Barrier (ETB), that reduces the rate at which particles radially escape the confined volume, improving the confinement in the process. The effect of the ETB is graphically described in Figure 2.5.

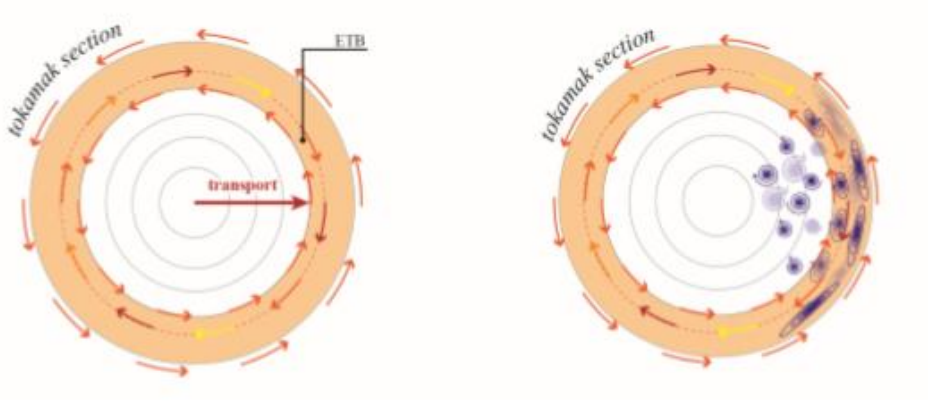

Figure 2.13 Effect of ETB on transport and turbulence

The rotation of the outer layers is differential, meaning that each radial position rotates with different speed, generating a gradient in angular velocity between them that is called a **sheared flow**. The shear acts on the **turbulent eddies** that radially transport particles out of the confinement volume, shearing and breaking them apart and, therefore, reducing the particle transport and improving significantly the confinement [17].

2.4.3 New variables and physical interpretation.

The sheared poloidal flow induced by the strong turbulence is the responsible for the appearance of the H-mode and the most important characteristic of the H-mode regime [18]. Therefore the sandpile features must be augmented in order to include a new dynamical variable, the shear. In the past, this has been done in the following way:

1. The shear is created by the turbulence, so the value of the shear at each cell is be increased when that cell becomes unstable and this is done according to rule 4.

   Rule 4: Each time a cell becomes unstable, its shear value is increased by ΔS.

2. When there is no turbulence, friction forces between adjacent rotating magnetic surfaces, tends to even out nearby rotating speeds, decreasing the shear of the flow. This process is introduced in the model by rule 5.

   Rule 5: In every iteration, if a cell does not become unstable its shear is reduced by dS.

   An important characteristic of the turbulence effect over the shear is that it drives shear significantly faster than friction forces reduce it, so it will always be assumed that $dS \ll \Delta S$.

3. Shear also affects turbulence by reducing it, that is enhancing the value of the required critical gradient, following rule 6, and therefore making more difficult for a cell to become unstable.

$$\text{Rule 6: } Z_c' = Z_c\left(1 + f\frac{S_n}{S_{max}}\right) \tag{2.2}$$

S_{max} represents the maximum shear that plasma is able to stand before becoming itself unstable. In a real tokamak, it would be related to a Kelvin-Helmholtz mode. The closer the shear is to its maximum, the greater the Z_c' and therefore the harder for a cell to become unstable.

4. Shear reduces the transport induced by the turbulence, so the number of grains transported to contiguous cells must be reduced according to rule 7.

$$\text{Rule 7: } N_f' = \frac{N_f}{\left(1+f\frac{S_n}{S_{max}}\right)} \tag{2.3}$$

When shear approaches its maximum value the transport of sand grains is minimized.

2.5 Shortcomings of this formulation for an H-mode cellular automata.

The previously described CA was firstly developed by UC3M Aerospace Engineering student Cristina Midori Fukuda under the supervision of Prof. Luis Raúl Sánchez Fernández, This implementation attempted to recreate some of the most characteristic features of the H-mode plasma such as the generation of shear by turbulence via the Reynolds stresses, and the action of shear on turbulence by the modification of the avalanching rules [19].

However, there is an ingredient that this implementation failed to achieve. It is known from experiments that in L-mode discharges fluctuations and their related transport exhibit very long memory. That is, the turbulent fluxes depend very strongly of the previous transport that has taken place in the system. In H-mode, however, this memory is strongly reduced and almost lost. In the CA implementation of the L-mode, memory is dominant in the system, with current avalanches strongly influenced by the previous avalanching history. This happens via the scars left in the sand profile by the passing of past avalanches, that have very long lives. In the H-mode CA implementation, this situation remains. Memory is still strongly active. This means that, although Cristina Midori Fukuda's CA model was a first step in the right direction, some characteristic features of H-mode transport were still missing.

3. MOTIVATION AND OBJECTIVES

The better confining properties provided by the H-mode regime increased the interest of the scientific community and the potential feasibility of fusion energy in electricity production. Specially from the 2020s, when ITER will start operating as an experimental reactor, properly designed simulation tools will be of great importance to help optimize and operate the experiment and help us find the most convenient way to design a real reactor.

The cellular automata approach discussed previously is an element that contributes to this effort of understanding the role that turbulence and shear play in setting the confinement properties of MCF fusion reactors. A fully-featured implementation of a H-mode cellular automata is still missing, as we discussed earlier, since the erasure of memory effects in turbulent transport by the action of the shear was not achieved. For that reason, the main motivation for this project is to analyze which elements must be added to fully incorporate this basic properties of H-mode transport and to implement them in a working CA that could be useful to better understand the dynamics and increase our predictive capabilities.

If successful this extended sandpile could be used as a simplified representation that captures the basic logic and the underlying mechanisms of the process under study. Moreover, it could set the basis for further mathematical and physical implementations to develop a three-dimensional model that defines both toroidal and radial directions, allowing the full recreation of the confining volume.

Therefore, the main steps of this project would be:

1. Design various extended sandpile models that progressively diverge from the original one by means of the introduction of new variables or relations in order to capture the missing features of H-mode transport.

2. Build a Matlab code that implements the new characteristics and exports results of the main variables involved in the transport dynamics.

3. Apply several analytical tools to characterize the results of the modified automata and compare them with those of the original implementation. In particular, we intend:

- Provide evidence of the reduction of the importance of avalanche memory in the dynamics. This will be done by analysing it using the Hurst Rescaled Range method.

- Characterize the changes in the causal relations between shear, turbulence and radial profile introduced by the new rules, through the use of the Transfer Entropy analysis.

4. MODIFIED SANDPILE MODEL

In order to succeed in capturing the memory suppression caused by shear on turbulent transport that is characteristic of the H-mode, some new rules have to be added or replaced that modify the system behaviour towards the desired features.

4.1 New automata rules

4.1.1 Randomizing the transport phenomena.

The previously explained rule 7, which stated that the value of Z_c is increased when shear approaches its maximum value, was introduced to capture one of the essential effects of the shear effect of reducing the turbulence: the reduction of the linear growth rate. However it does not reduce the importance of the memory of previous avalanches on future relaxations. For that reason, it was decided to be replaced by a new rule inspired by the particle physics occurring at the micro-scale .

The appearance of a stable shear flow is known to affect the turbulence mainly through the distortion of the turbulent eddies, changing their characteristic scales in space, time and amplitude [20].

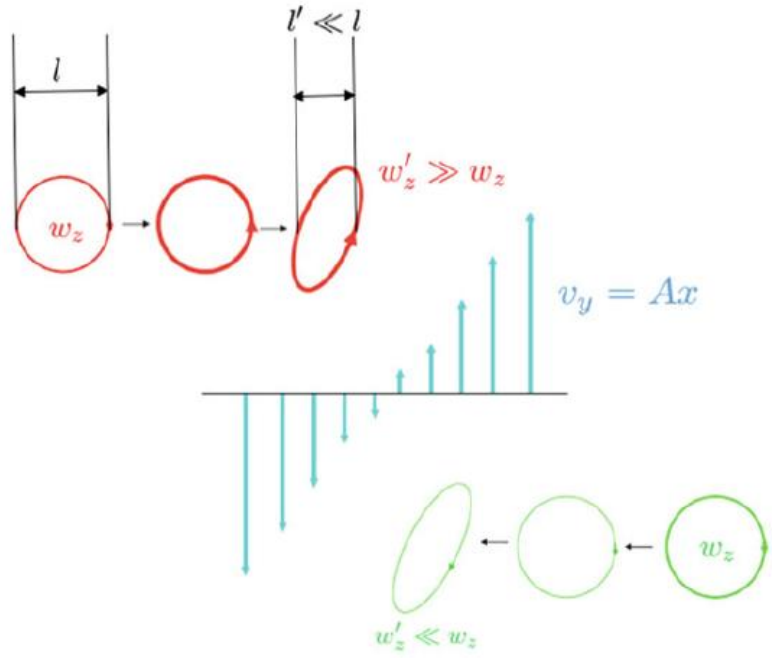

Figure 4.1 Action of shear flow on eddies containing vorticity of different sign.

As shown in Fig 4.1, the characteristic size of the eddies across the flow could be significantly reduced and, depending on its vorticity sign, the local rotational speed can be enhanced (in red) or reduced (in green). Both characteristic changes could induce a reduction of the lifetime of the turbulent vortices conforming a turbulent flow, since the

life of an eddie is defined as the time needed by its neighbouring eddies to shear it apart. The reduction in the characteristic size, the possible increase of local rotational velocity of its neighbours and the stretching of the vortex structure might enhance the influence of the nearby eddies, causing a faster and stronger widening, reducing significantly the lifetime.

But the opposite circumstance is also possible, being the shear flow of opposite sign to the rotation of the neighbours, reducing their rotational velocity, and the stretching and size reduction could allow a particular eddie to escape from the influence domain of the adjacent vortices, allowing longer lifetimes.

In accordance to this, a new variable called "P_k" was added to the model, in order to regulate the probability at which particles move radially from one magnetic surface to another. If the turbulent eddy responsible of radially transporting a particle suddenly vanishes, the particle will not cross the magnetic surface boundary and will still be confined. The value of this probability has to decrease with the shear being close to its maximum value, because eddies are more easily destroyed by larger shear values, according to new rule 7.

$$\text{Rule 7: } P_k = P_1\left(1 - \frac{S_n}{S_{max}}\right) + P_2 \tag{4.1}$$

Three pairs of values for P_1 and P_2 were analyzed, each pair summing 1 as maximum P_k if no shear was present and having $P_k = P_2$ in case the shear is maximum. The first pair would be $P_1 = 0$ and $P_2 = 1$, corresponding to the basic case where the probability of occurrence is not affected by the shear. The second case presents $P_1 = 0.2$ and $P_2 = 0.8$ and the third uses $P_1 = 0.5$ and $P_2 = 0.5$, therefore progressively reducing the value of P_k at maximum value of the shear and moving away from the basic case and introducing the dynamics of a more randomized behaviour.

4.1.2 Eliminating long-term memory

In Cristina Fukuda's original H-mode CA model the profile was always **locally subcritical**. That is, avalanches take place when the profile surpasses the critical gradient. But they do it so quickly that, on average, the sustained profile is below the local threshold. In this regime, the subcritical profile can store memory of the past avalanches, since they leave a trace when changing the profile local values that conditions the appearance of future avalanches.

This memory effect can be removed (or at least ameliorated) by making avalanches much more frequent and pushing the profile to an average **supercritical state**. In this way, traces of past avalanches disappear quickly and memory cannot be sustained for long [21]. A supercritical profile can be reached by enforcing a new rule 8. That is, choose parameter values such that:

$$\text{Rule 8: } P_o N > \frac{N_F^{'}}{2} \tag{4.2}$$

In order to fulfil rule 8 any and to avoid substantial increases of the compiling time, the modified variable is f in formula $N_f^{'} = \frac{N_f}{(1+f\frac{S_n}{S_{max}})}$.

Achieving a low value of $N_f^{'}$ in the near maximum shear region. Three values of f were selected for the further analysis f=0.2, corresponding to the basic scenario, and f=10 and f=20 to progressively diverge from the basic scenario.

TABLE 4.1. IMPLEMENTATION OF SHEAR-RELATED RULES

Rule number	**Physical processes**	**Sandpile implementation**
Rule 4	Turbulence causes shear	If a cell becomes unstable, shear at that cell is increased by ΔS
Rule 5	In case of no turbulence, friction forces reduce the shear	If a cell does not become unstable shear is lowered by dS
Rule 6	Shear reduced the transport induced by the turbulence	Value of Nf diminishes as shear approaches Smax
Rule 7	The turbulent eddies can be vanished by the shear, slowing down the transport	Pk ultimately determines if transport occurs even if the rest of conditions are favourable
Rule 8	Shear reduces the long-term memory of the plasma	f values are increased so system becomes locally supercritical

4.2 Modified algorithm

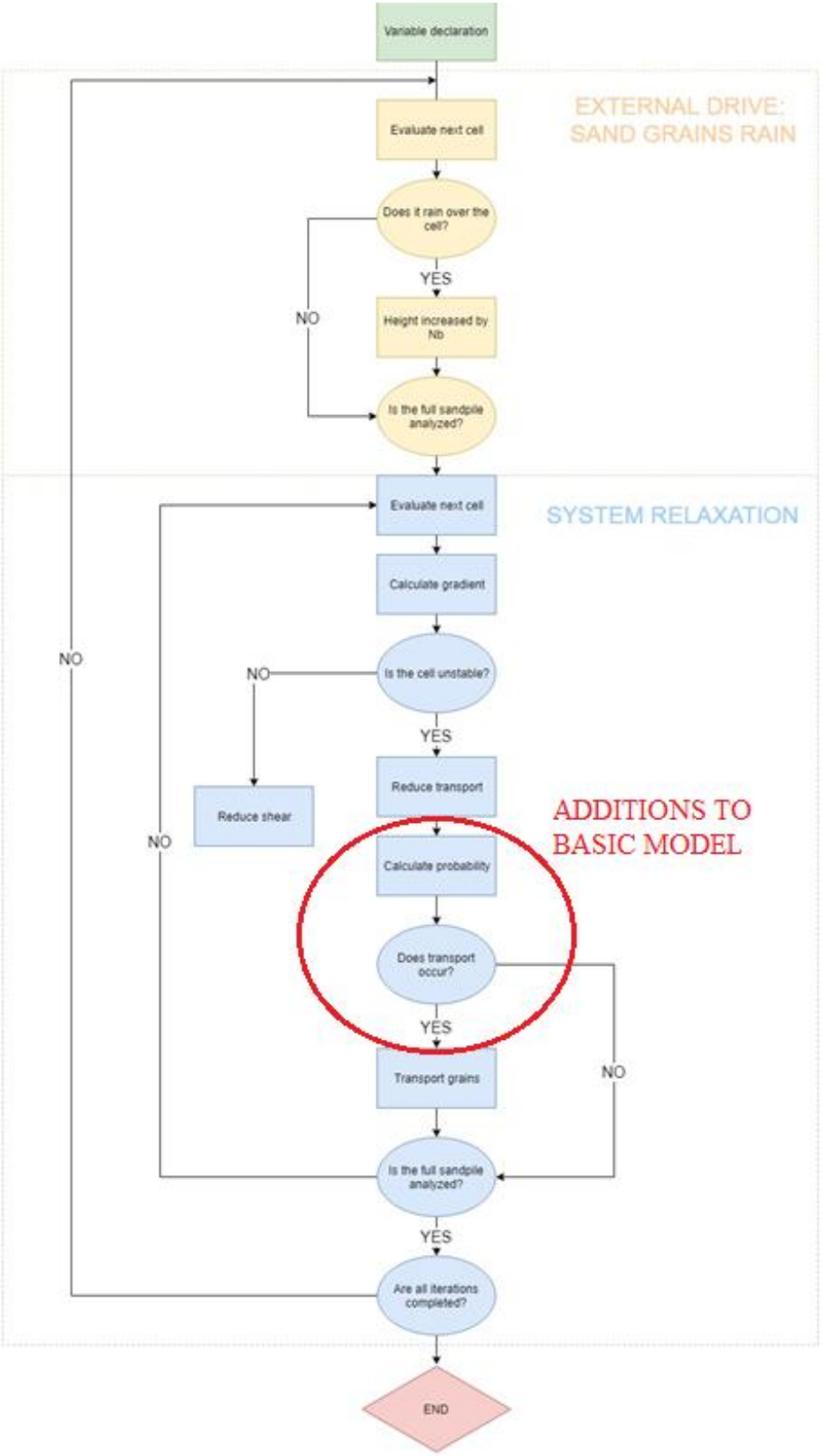

Figure 4.2 Flowchart of extended sandpile model algorithm. Changes caused by the Introduction of new rules 7 and 8 are represented inside the red circle

4.3 Example of the modified sandpile model run

TABLE 4.2. VARIABLES IN THE MODIFIED SANDPILE MODEL

Name	Value	Meaning
N	200	Sandpile cells
P_0	10^{-3}	Rain probability over each cell
N_b	1	Grain rain on each cell
Z_c	200	Critical threshold
N_f	20	Grains transported from a unstable cell to the adjacent
f	**20**	**Regulator of shear effect over N_f**
S_{max}	20	Maximum possible value of shear
dS	10^{-3}	Shear decrease if cell is below threshold
ΔS	0.1	Shear increase if cell becomes unstable
P1	**0.5**	**Regulator of shear effect over transport probability**
P2	**0.5**	**Independent component of transport probability**

The highlighted values have been chosen to take the system to a regime in which supercriticality can exist on average. In this way, we will be able to compare the effect of the new rules with the original H-mode CA model. In particular, we will analyse the following elements:

i) SOC state achievement

ii) Radial shear distribution

iii) Gradient profile at the steady state

iv) Turbulent activity.

4.3.1 SOC state achievement & radial shear distribution.

The modified sandpile just described is run to saturation starting from a maximum value of the shear, $\mathbf{S}_n = 20$ in each cell, and a local gradient equal to the critical threshold, $Z_n = 200$. In this way, the system is way supercritical everywhere, avalanche activity will be very strong, and the stationary SOC state is reached earlier.

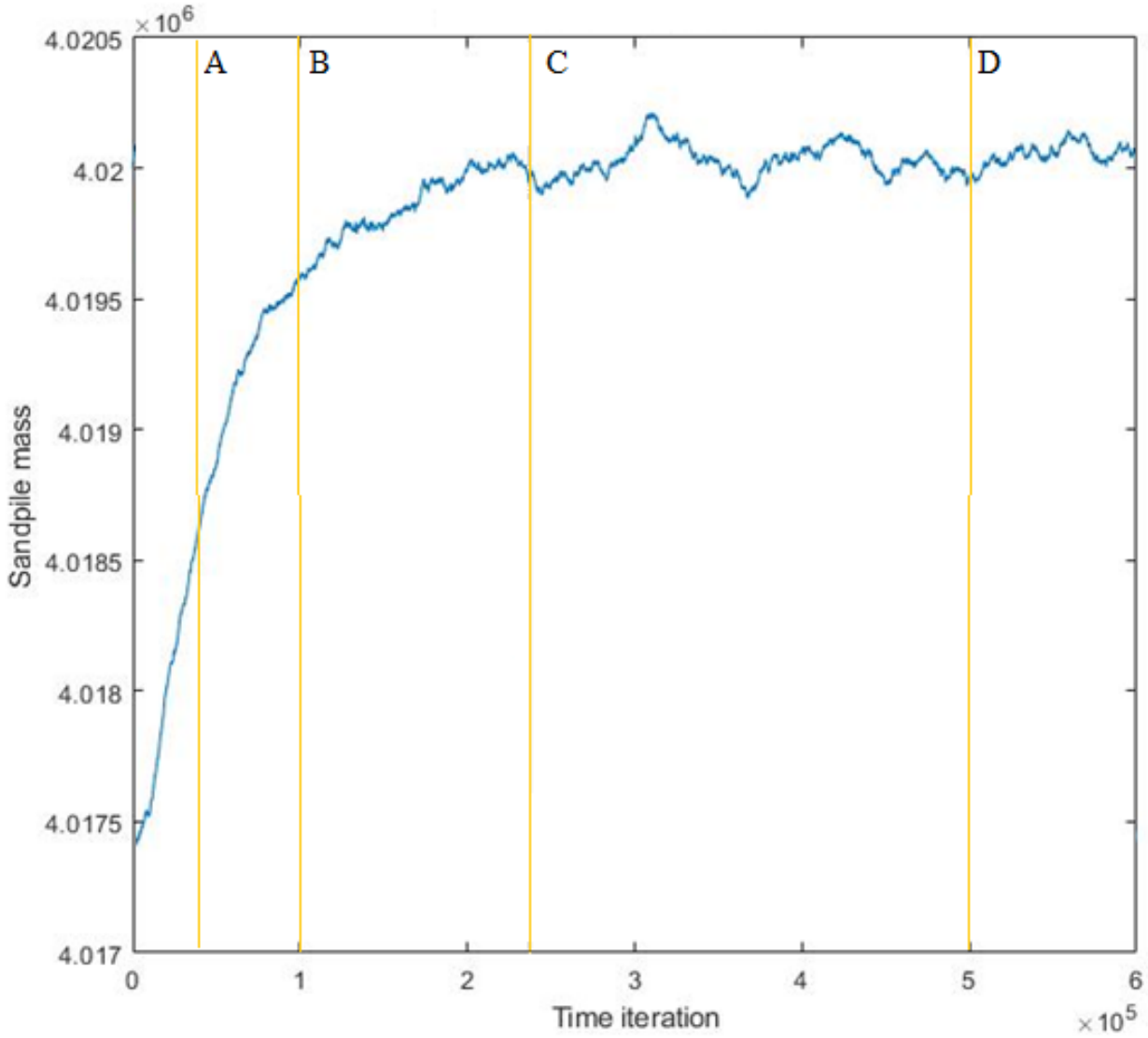

Figure 4.3 Evolution of sandpile mass from near critical conditions with SOC state achievement. Four specific time moments are highlighted for further analysis (A, B, C, D)

As stated before, the SOC state is reached when the mass escaping the sandpile balances the mass addition from the rain, achieving a total mass profile that fluctuates around a constant mean value. The saturation of the profile shown in Figure 4.4. Reaching this state is critical before any data extraction from the model, since the further analysis requires the studied variables to be stationary time series and that is only possible if the profile is saturated.

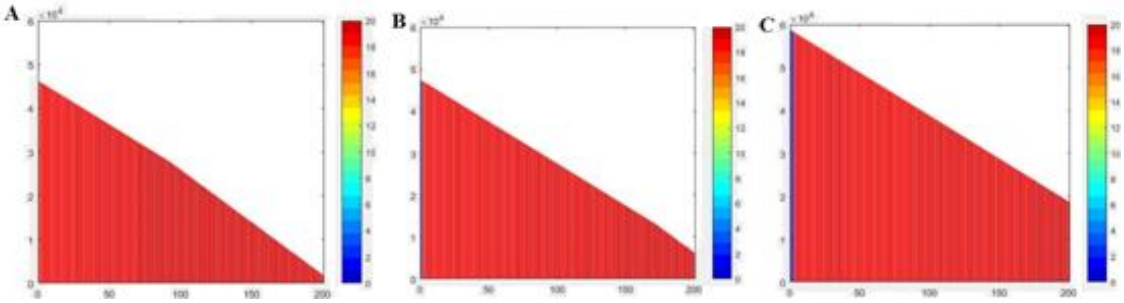

Figure 4.4 Shear and profile evolution of supercritical H-mode sandpile model. The color legend at the right corresponds to the shear value, being red when maximum and blue when equal to 0.

It can be seen that, from A to B, the profile becomes steeper in the right half of the profile, due to the evolution of the shear to reach its maximum value in the whole sandpile.

In C the first cells at the left achieve a shear value of 0 and a pedestal is generated keeping the profile stiffness but rising it, increasing the total mass of the system and reaching SOC state at this moment.

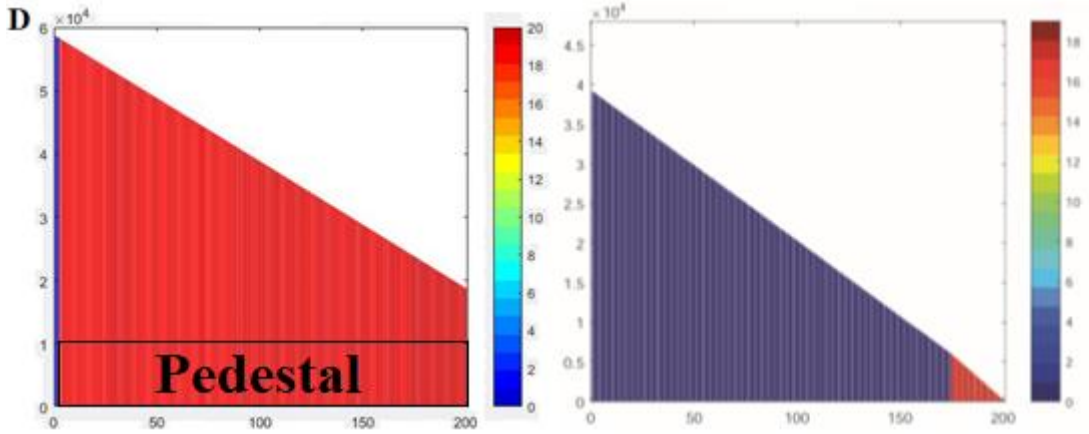

Figure 4.5 Shear and profile comparison between supercritical (left) and basic model (right)

The profile at D is found to be equal to the one presented in C, even though they are 2.5×10^5 iterations apart. This is the basic dynamic of the SOC state, where the profile seems invariant to changes induced from the external source, since all the mass that enters the sandpile is exerted in the following iteration.

When comparing the profiles of the new and the original CA models (see Fig. 4.5), two main differences become apparent:

- The value of the shear is maximum in almost the entire sandpile in the supercritical regime, while in the subcritical, all the system has been relaxing and when the SOC state is reached only a slight part at the end of the sandpile is having shear, while the most part presents a value of 0 (blue color).

- The mass profile of the supercritical regime is raised by the appearance of the pedestal at the lowest part of the profile, while in the subcritical, the pedestal is much weaker, appearing as a simple larger gradient.

4.3.2 Gradient profile & avalanching activity.

In the original CA model rule 8 was not implement and, therefore, the gradient profile remains on average below the critical threshold. Figure 4.6 shows the gradient profile at one time iteration of the original CA model, clearly showing a **locally subcritical** system. In fact, it can be seen that the critical Z_c value is only exceeded at one cell. This would produce an avalanche, starting in this cell and propagating to the right until the profile of one of the following adjacent cells is more than Nf' grains below the threshold, so that the sand addition from the previous one does not cause it to be unstable.

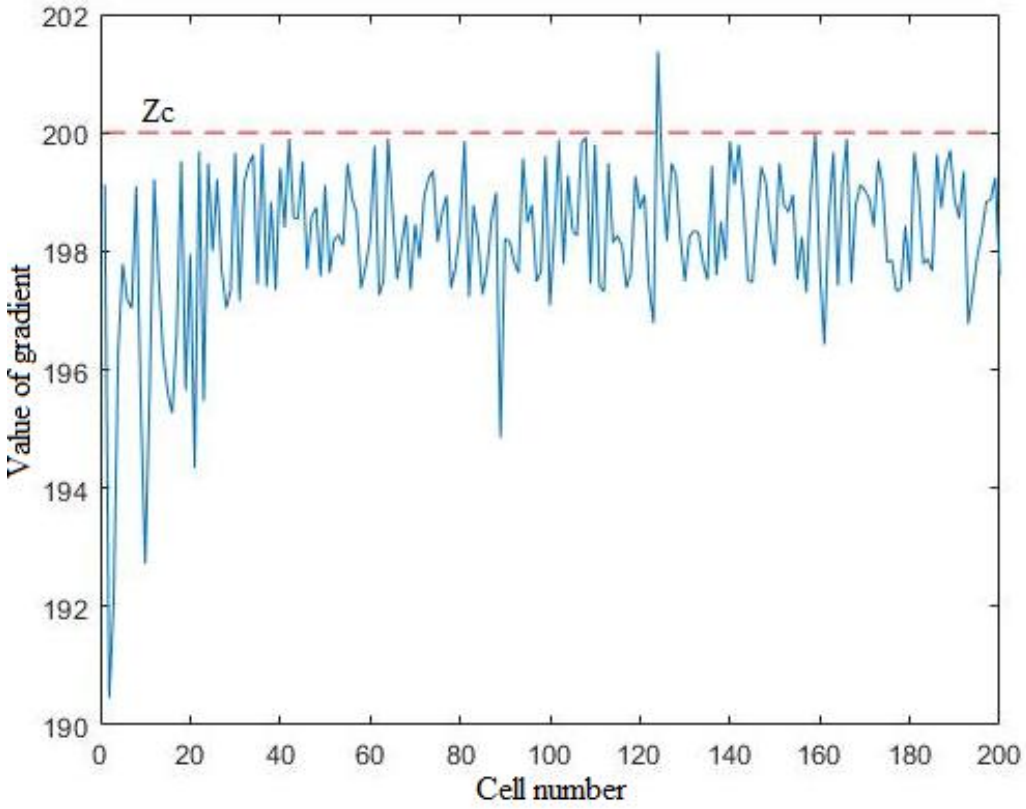

Figure 4.6 Subcritical gradient profile

Avalanches in subcritical profiles continuously set the profile below threshold, making all the sandpile unstable cells back to stabilization, therefore setting the activity to a value of 0. This behaviour can be seen in Figure 4.7, since all values of activity are annulled before rising back again, this is all unstable cells are stabilized before becoming unstable again by the external rain. Moreover, Figure 4.7 also slightly reflects the avalanche memory of subcritical regimes, since previous avalanches generate the following ones and the profile shows differentiated areas of calm and high activity.

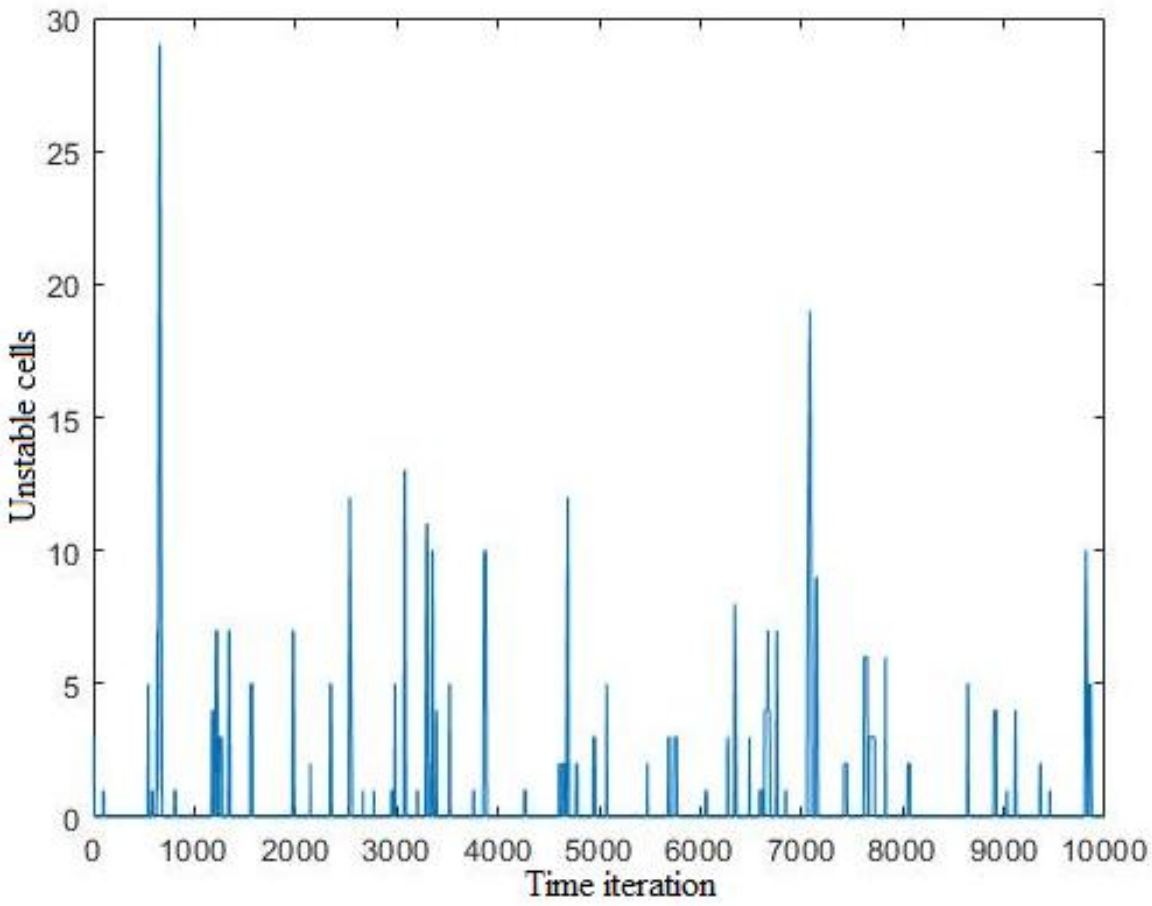

Figure 4.7 Activity regime in subcritical gradient profiles

In contraposition to the subcritical regime, the implementation of rule 8 induces significant changes in the behaviour of the profile. Figure 4.8 shows the resulting gradient profile, typical of a **locally supercritical** system. In it, the sandpile cells are subjected to maximum values of shear and have slopes constantly above the critical threshold. As a result, there is a large number of unstable cells and consequently many avalanches starting in each iteration. In this regime, the Nf' value is so low and the number of unstable cells so high, that is impossible for the avalanches to reduce the profile below critical quickly enough.

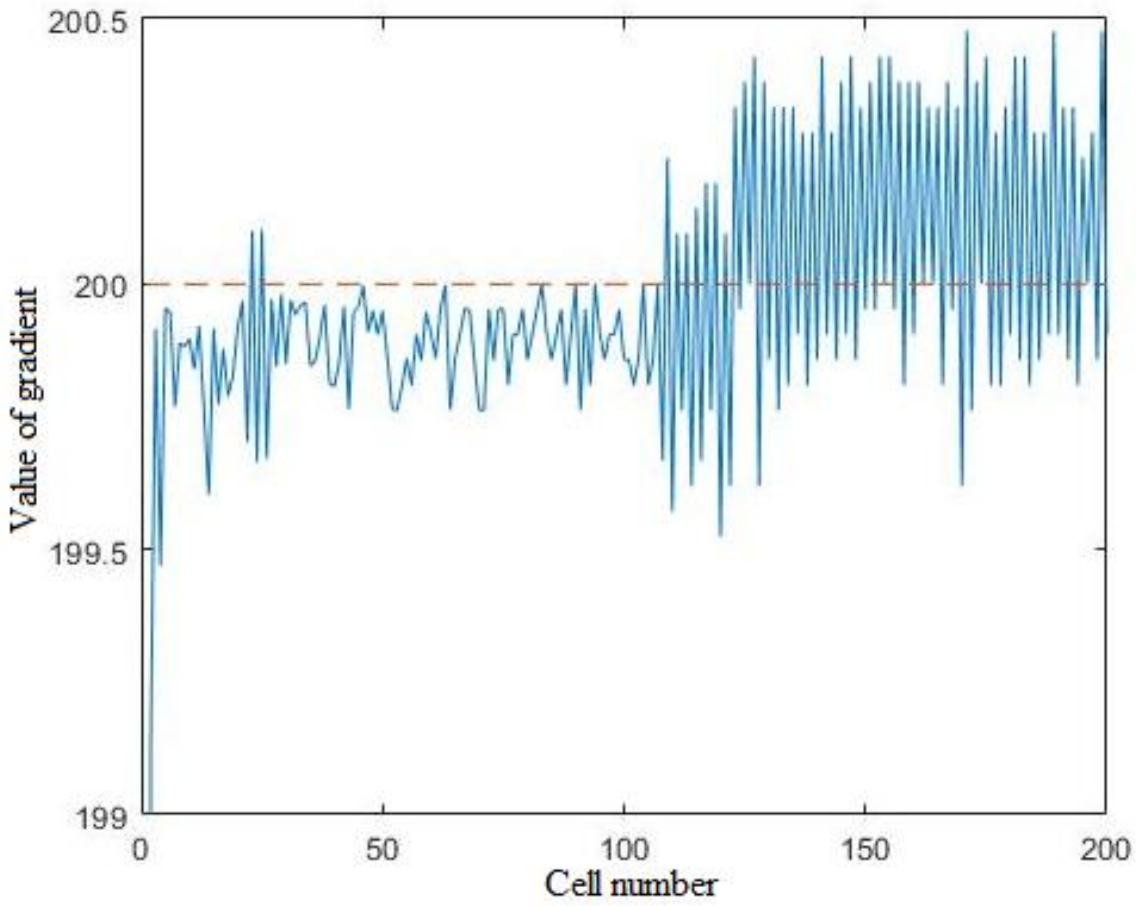

Figure 4.8 Supercritical gradient profile

Therefore, large quantities of avalanches are started in the maximum shear region, keeping always a high activity. This is seen in Figure 4.9, in which sandpile avalanche activity fluctuates around a high value and the 0 value is no longer reached. Moreover, a minimum of nearly 60 cells are unstable in every iteration, more than doubling the maximum activity of the subcritical regime. Memory could be reduced due to the high amount of avalanches, that erase the traces from the previous ones. However, this can not be concluded merely by observing the activity regime and analytic methods must be applied in the following section to assure the proper functioning of the newly implemented model.

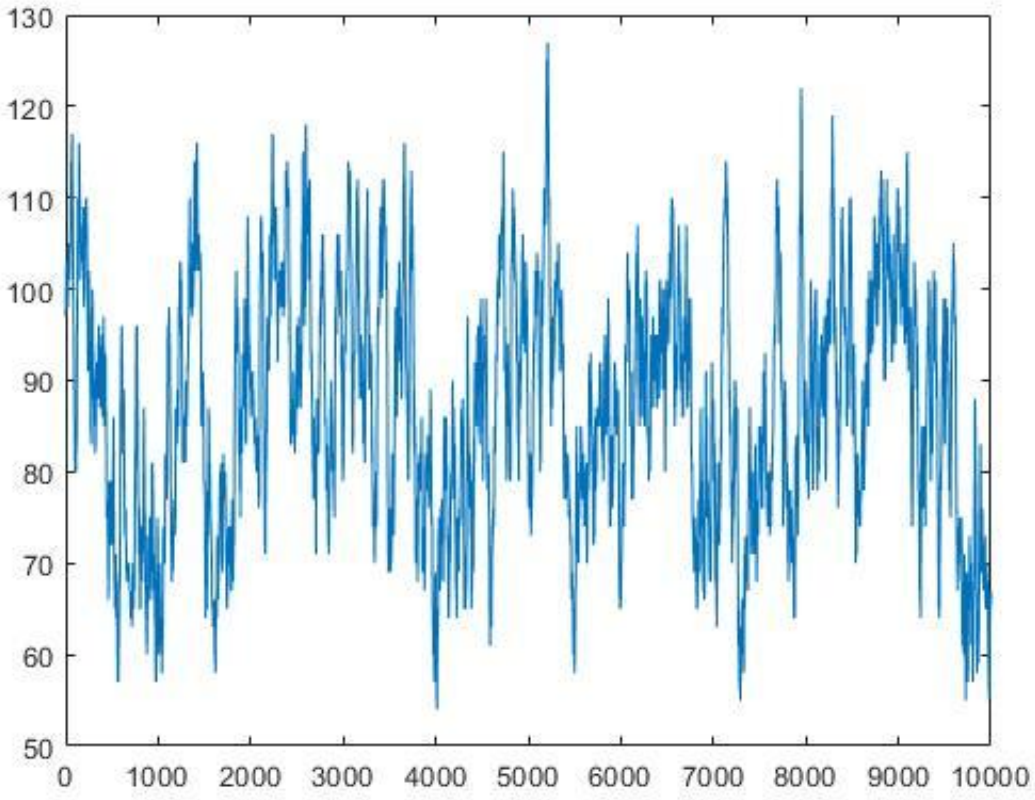

Figure 4.9 Activity regime in supercritical gradient profiles

5. ANALYSIS OF RESULTS

5.1 Hurst's Rescaled Range (R/S) method.

The R/S method is a well known statistical method to detect the presence of memory in time series.

5.1.1 Definition of Hurst's Rescaled Range.

R/S method is an analytical tool first introduced by Harold E. Hurst in the 1950s while studying the long-term dependencies in the water content of the river Nile [22]. It must be applied on a *stationary time series* as follows:

1. The series is demeaned:

$$\widetilde{y_k} = y_k - \frac{\sum_{i=1}^{N} y_i}{N} \tag{5.1}$$

2. The demeaned vector is cumulative summed:

$$z_k = \sum_{i=1}^{k} \widetilde{y_i} \ , k = 1,2, \dots . , N \tag{5.2}$$

3. The standard deviation is calculated:

$$\sigma_k = \sqrt{\frac{1}{k}\sum_{i=1}^{k} \widetilde{y_i}^2 - \left(\frac{1}{k}\sum_{i=1}^{k} \widetilde{y_i}\right)^2} \tag{5.3}$$

4. The *rescaled range* is defined as:

$$(R/S)_k = \frac{max\{z_i, i = 1, \dots k\} - min\{z_i, i = 1, \dots k\}}{\sigma_k} \tag{5.4}$$

5. The Hurst exponent ($H^{R/S}$) is derived from:

$$(R/S)_k \sim k^{H^{R/S}} \tag{5.5}$$

Essentially, the R/S method measures the range of values examined by the process along the first k iterations normalized to its standard deviation, in order to spot the long-term dependence of the signal and detect memory in *stationary time series*. Being the value of the Hurst exponent the key indicator to address the type of time dependence.

If long term correlations were present in the signal a value of $H^{R/S} \neq 1/2$ would be found. More precisely, if the correlations were positive, the increments should tend to maintain their sign more often than changing it, and the range would grow faster with k.

In other words, $H^{R/S} > 1/2$, with a limiting value of 1, corresponding to a constant series. On the other hand if correlations were negative, $H^{R/S} < 1/2$ would follow, with a limiting value of 0.

For completely random signals exhibiting no memory, $H^{R/S} \sim 1/2$ would hold.

5.1.2 Hurst's Rescaled Range analysis of the new H-mode sandpile model.

In order to perform this analysis, several sandpile cases were saturated until SOC state was reached, including one that followed closely the original implementation by Cristina Fukuda. Three main representative variables were extracted in each run for further analysis:

- The **avalanching activity**: as stated before, it is the total number of unstable cells in the sandpile at each iteration.

- The **instantaneous variance of the shear** (σ_{shear}): the shear is the most important characteristic of the H-mode. However, its value is different for each cell and changes each iteration. The instantaneous variance is computed to provide a global measure of the shear dynamics relevance at each iteration.

$$\sigma_{shear} = \sqrt{\frac{1}{N}\sum_{i=1}^{N}\left(S_{n_i} - \frac{1}{N}\sum_{i=1}^{N} S_{n_i}\right)^2} \tag{5.6}$$

- The **instantaneous variance of the gradient** ($\sigma_{gradient}$): the gradient is the variable responsible for the occurrence of the transport phenomena and must be accounted in this analysis. The same procedure of the shear is applied to the gradient variable,

$$\sigma_{gradient} = \sqrt{\frac{1}{N}\sum_{i=1}^{N}\left(Z_{n_i} - \frac{1}{N}\sum_{i=1}^{N} Z_{n_i}\right)^2} \tag{5.7}$$

Once the sandpile reaches the SOC state, a sufficient long time series is extracted for these three variables, the R/S analysis is performed for each one. The results for the avalanching activity have been found to be the most representative in order to characterize the differences between the subcritical regime of the original CA and the supercritical regimes of the new implementation.

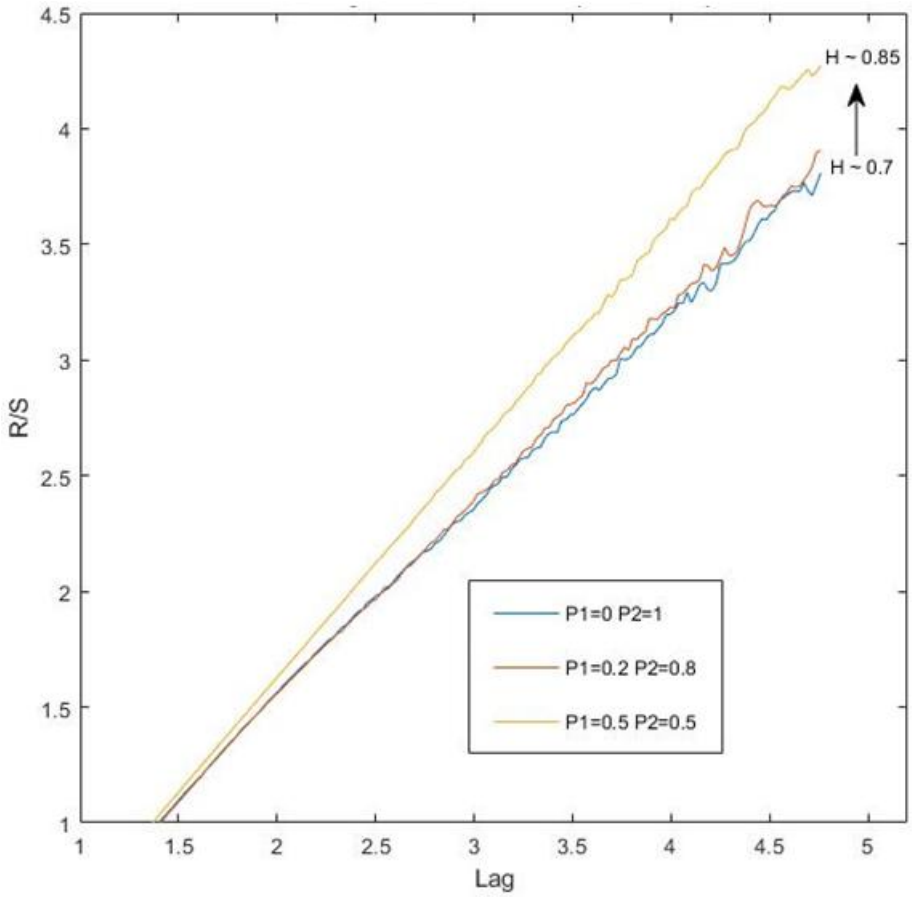

Figure 5.1 Hurst Rescaled Range of the activity of a subcritical profile (f=0.2)

In the case of the original CA with subcritical profile (where only rule 7 is used), the variation of the probability pair (p1, p2) increases the value of the Hurst exponent from 0.7, for the original case, to 0.85, as seen in Figure 5.1.

As explained before, values of Hurst exponent above 0.5 mean that memory is present in the signal, the more the closer to unity. This happens because the further from the original case the harder it is for avalanches to occur, even if the cell is unstable and the conditions for the avalanche occurrence are fulfilled. But this does not erase the effect of avalanching on the profile, since they only determine the probability of transport to happen. In the extreme case of $P_1 = 0.5$ and $P_2 = 0.5$, for the cells having maximum values of the shear, only 50% of the avalanches that are meant to happen will actually take place. Thus, past tracers will stay longer, not less in the system and long-term memory, as a result, increases.

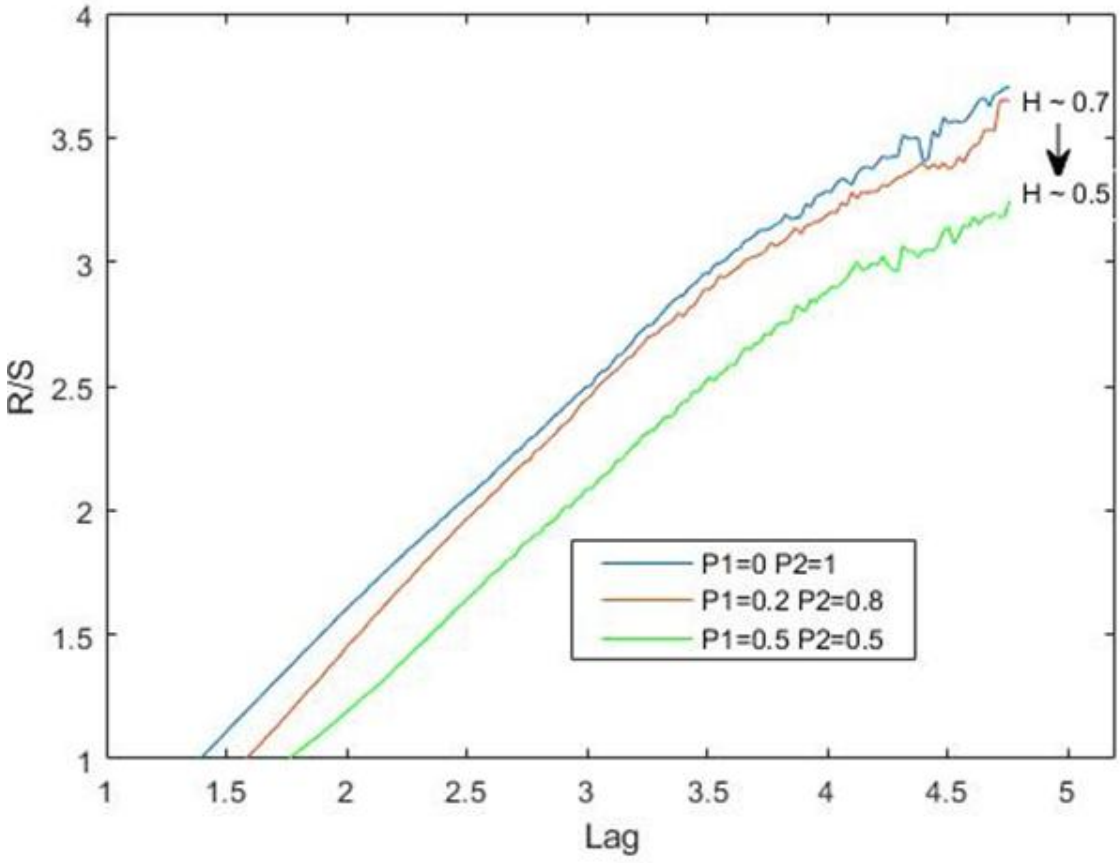

Figure 5.2 Hurst Rescaled Range of the activity of a supercritical profile (f=20)

In the modified CA model, where a supercritical profile appears due to the application of both rules 7 and 8 are fulfilled, the value of the Hurst exponent at the longest lags evolves from a value of 0.7 to 0.5, as seen in Figure 5.2. This is the behaviour that we were looking for.

The approximation of H to 0.5 means that the time series becomes more uncorrelated, since a pure random walk would lead to an exact value of 0.5.

This state of things is reached due to the high activity of the maximum shear region, which erases the influence of previous avalanches in the actual transport dynamics of the profile. Making the actual and further avalanches independent from their past history significantly decreases the memory of the sandpile and progressively approaches a profile where only present characteristics of the sandpile are taken into account and where avalanches are much more randomly triggered.

5.2 Transfer entropy

In the original sandpile studied by Cristina Midori, the transfer of net entropy was used to establish the causal relationships between avalanches, shear and profile modification. In this section we characterize the new causal relationships that are established because of the application of the new rules, and compare them with those in Midori's CA.

5.2.1 Definition of Transfer entropy

Transfer entropy is a non-parametric statistical tool that can be used to analyze causality between time series. It was first introduced by Thomas Schreiber in year 2000 [23] in the following way: "For two simultaneously measured signals X and Y, if we can predict X better by using the past information from Y than without it, then we call Y causal to X".

The mathematical procedure is simple and summarized in the following expression, where X and Y are two different variables whose time series is constituted by $x_i$and y_i are meant to be analyzed. To quantify to what extent changes in Y induce changes in X, that is X is caused by Y [24]:

$$T_{Y\to X} = \sum P(x_{n+1}, x_{n\text{-}k}, y_{n+k}) log_2 \frac{P(x_{n+1}|x_{n\text{-}k}, y_{n+k})}{P(x_{n+1}|x_{n\text{-}k})} \tag{5.8}$$

Here k represents the time lag between the two time series being compared. By changing this lag one can detect the mutual influence at different time delays, since causality may be instantaneous or take some time, or even change direction at different timescales.

$P(x_{n+1}|x_{n\text{-}k})$ expresses a conditional probability: "the probability of occurrence of A if B has occurred". In case that y_{n+k} does not affect the probability of x_{n+1}, the following equation will hold $P(x_{n+1}|x_{n\text{-}k}, y_{n+k}) = P(x_{n+1}|x_{n\text{-}k})$, simplifying the fraction and making the logarithm and therefore the transfer entropy equal to 0.

For this study, the concept of **net transfer entropy** is used, that is calculated as:

$$T_{Y\to X}{}^{net} = T_{Y\to X} \text{-} T_{X\to Y} \tag{5.9}$$

$T_{Y\to X}{}^{net}$allows to detect the direction of the causality. When being positive Y would be the cause of X and when negative the opposite would happen. If the net transfer entropy is found to be 0, when its constituents are not, this would mean that both variables affect each other in similar ways or are completely independent of each other.

5.2.2 Transfer entropy analysis of the original H-mode sandpile.

The variables analysed are the same that were used in the Hurst (R/S) analysis. That is, the avalanching activity, the instantaneous variance of the shear of the flow and the instantaneous variance of the gradient.

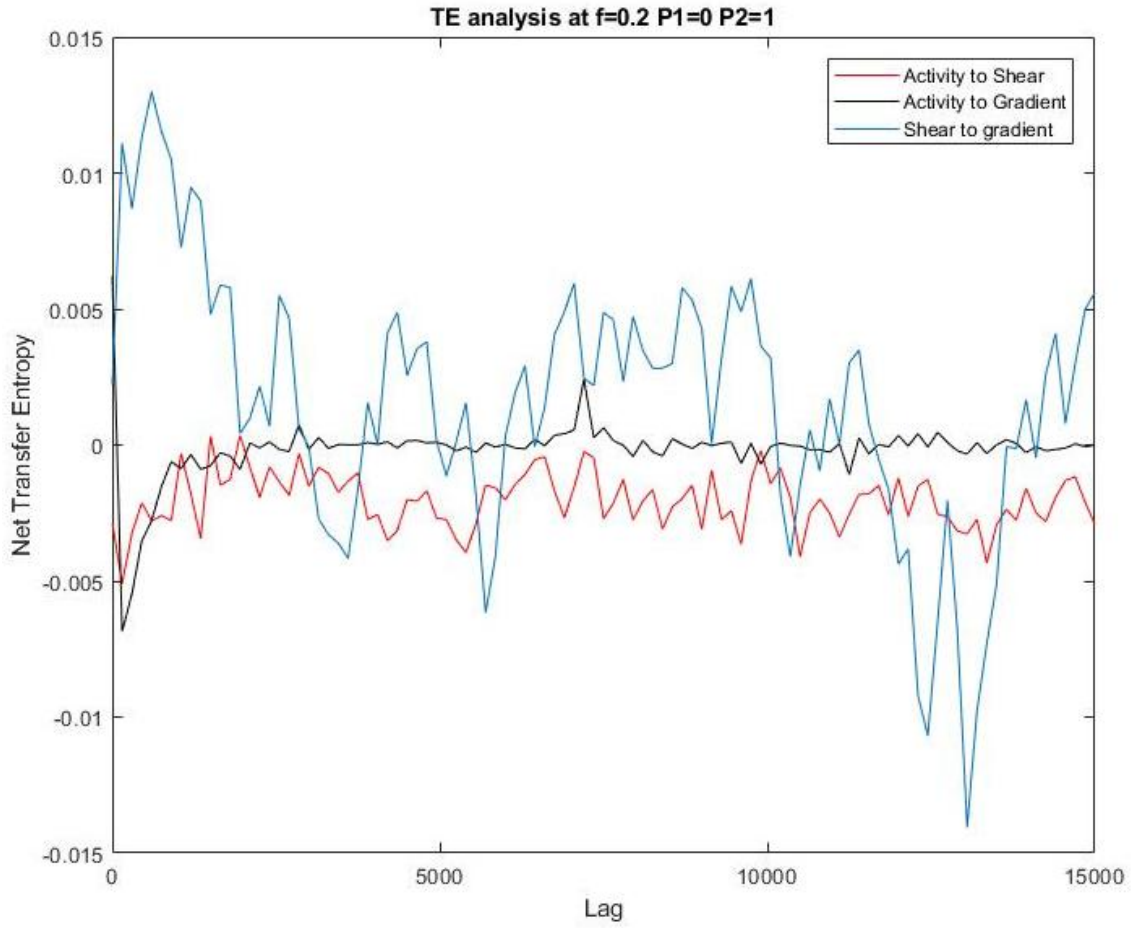

Figure 5.3 Transfer entropy evolution of the basic case (f=0.2 P1=0 P2=1)

As explained before, a positive value of the net transfer entropy means that the transfer (and thus the causal relationship) occurs in the direction shown in the legends of the figure, while for a negative value, the transfer reverses this direction.

Figure 5.3 exhibits the following features:

- At short times (~500 iterations) there is a large positive net entropy transfer from "Shear to Gradient". This means that shear conditions the dynamics of the gradient and gradient values could be better predicted if knowing the previous shear state.

- The dominance of the shear over both other variables is present along all evolution, being significantly greater when causing the gradient than the activity. This is because shear is highly and rapidly increased when instabilities appear but very slowly reduced, taking many iterations, due to friction forces. This causes the shear to have significant values during most of the evolution, therefore conditioning the other variables.

- It is also seen that, for short times, there exist a causal flow from the gradient to condition the activity, that later vanishes at further iterations. This is a natural consequence of the fact that avalanches are trigger after the gradient becomes sufficiently large.

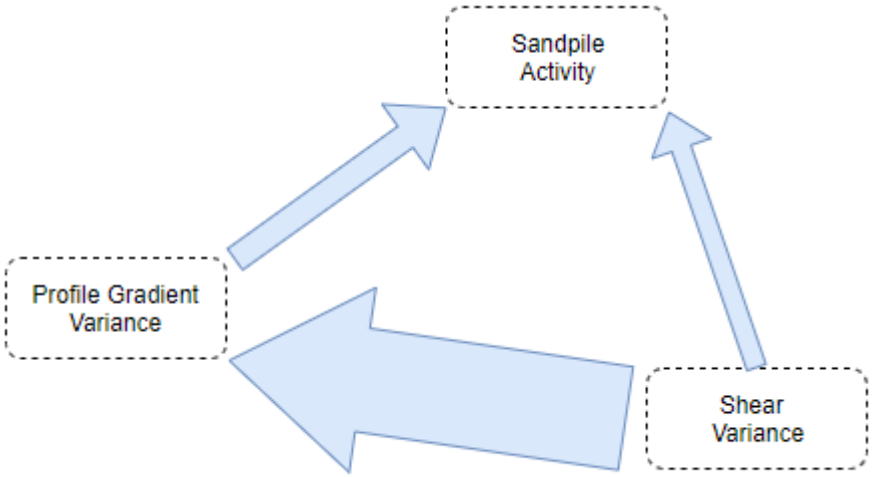

Figure 5.4 Transfer entropy causal flows in the original H-mode running sandpile.

The results obtained can be summarized in a typical arrow-transfer-plot (ATP), as the one shown in Fig. 5.4. Its interpretation tells us that:

- Shear causality over the gradient is greater at short term and found to be the dominant drive during the whole evolution. Therefore, it is the shear values that rapidly condition the sandpile profile.

- Shear also conditions the activity of the avalanches during all the evolution but more weakly than the profile changes, since it modifies the flux they can carry (through the changes in the value of Nf).

All in all, the shear is proved to be the primary factor conditioning the transport dynamics in the basic H-mode, since it conditions the other two variables while not been conditioned.

5.2.3 Transfer entropy analysis of the modified H-mode sandpile.

In order to see the effects of the substitution of rule 7 and the introduction of rule 8, the Transfer Entropy analysis is performed on the most supercritical case previously described. The results of the analysis are shown in Figure 5.

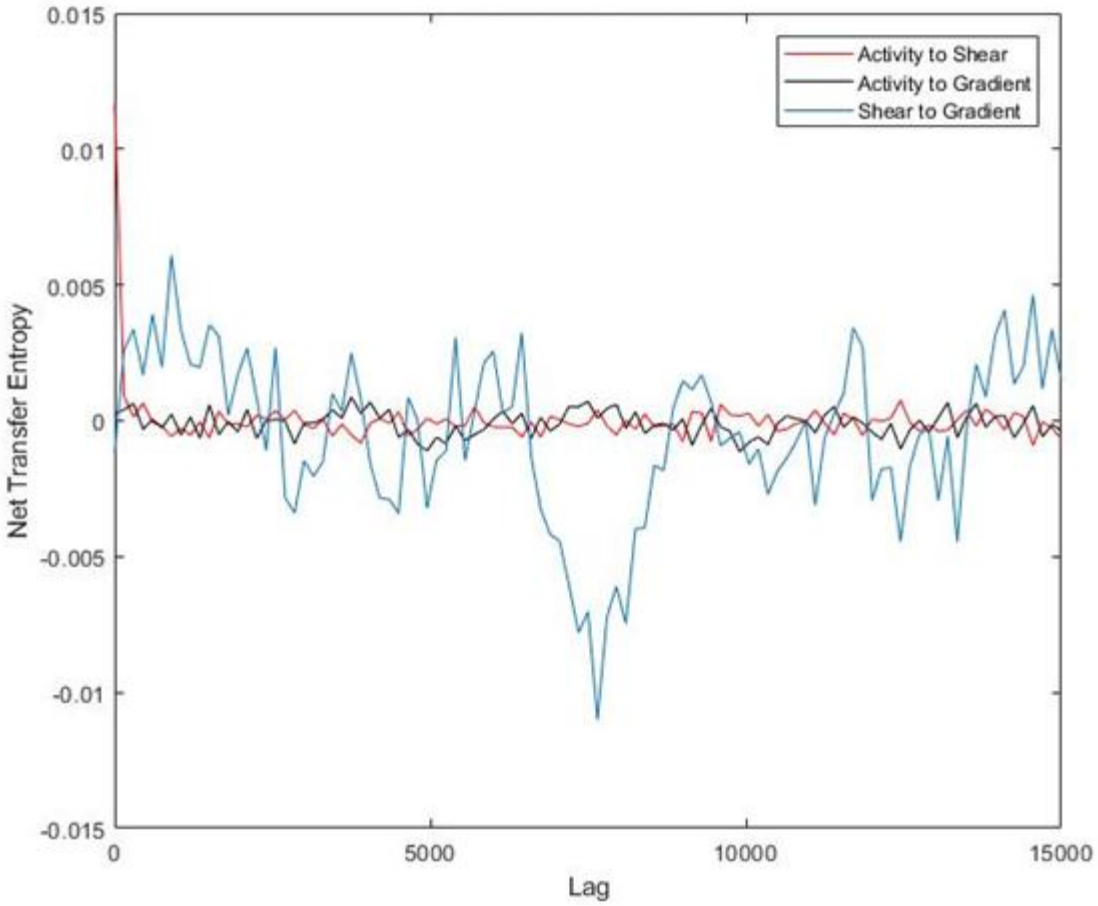

Figure 5.5 Transfer entropy evolution of a supercritical case (f=10 P1=0.5 P2=0.5)

Figure 5.5 provides evidence of the following characteristics, in comparison with the original CA, whose results for the same analysis were shown in Figure 5.3:

- The shear dominance over the gradient is still present during the complete analysis, but with significantly reduced intensity, particularly in the short term, when compared to the original case.

- Activity is now found to heavily condition the shear only at the start of the evolution, while later both variables became much more independent. This is an important change in comparison with the basic model behaviour, where shear conditioned activity at almost all times. This is clearly a consequence of the fact that avalanches are active most of the time, which reduces the impact of the shear on profiles due to the much shorter (if any) waiting-times between avalanches.

- Avalanche Activity no longer affects the gradient dynamics at short times, as in the original model, now they are proved to be independent during at any time. The reason for this is also clear; avalanches are no longer efficient enough to stop transport and to flatten the profiles back to stability. As a result, the evolution of the profile is more conditioned by the strength of the drive, which is in itself random.

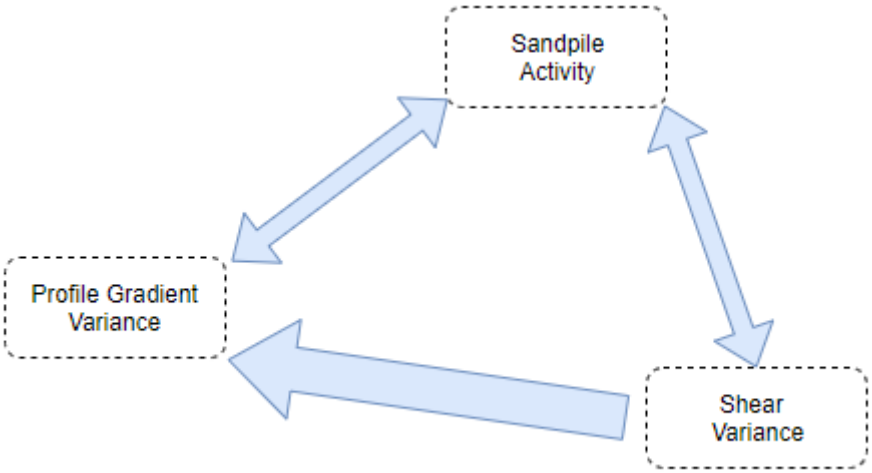

Figure 5.6 Transfer entropy causal flows in the supercritical H-mode running sandpile.

If we build the arrow-transfer-plot in this case it would look like the one shown in Fig. 5.6. The dynamical implications from the plot are:

- Shear is still the dominant variable, with a significant effect over the gradient profile but reduced effect over the activity.

- Avalanche activity and gradient seem to be independent due to the constant avalanching being present, at the high shear region of the sandpile, which is never efficient enough to control the profile shape. The reduction in memory previously discuss is also a consequence of this, as shown in the Hurst exponent analysis.

6. CONCLUSIONS AND FURTHER WORK

The main conclusion of this project is that we have been able to modify and extend the set of rules that defined C. Midori's H-mode Cellular Automata (CA) in order to overcome some its shortcomings to capture the basic dynamics of turbulent transport in H-mode tokamak plasmas. In particular, the fact that memory still remained dominating the temporal dynamics of the system after the introduction of the shear. By changing some of the rules to drive the pedestal region into the supercritical regime, memory has been effectively erased and the CA dynamics have become much closer to what is seen in tokamak experiments.

These results have been characterized by means of two statistical tools: the R/S Hurst analysis and the transfer entropy analysis. The latter had been previously used by C. Midori to characterize her modified H-mode sandpile, but the Hurst analysis was not. Hurst analysis of the avalanching activity in the modified CA clearly shows the loss of memory at the longer timescales, as needed. In addition, the transfer entropy analysis shows that the role of shear, although still dominant, is quite different and more consistent with the loss of memory previously discussed. In addition, avalanches are not able to condition the profile evolution as tightly as in Midori's case due, among other things, to the fact that supercriticality is obtained by reducing the power of avalanches to flatten the profile locally to stability.

The cellular automata developed in this project has been implemented from scratch using Matlab. The program created, recreates the essential logic and basic transport mechanisms present in a real reactor, while characterized by its simplicity and very intuitive approach. The data extraction tools that have been developed for this work within the Matlab framework are also very clear and easy to use, providing the required amount of information needed to understand the changes in the different involved variables and to develop the required analysis.

The procedures introduced and implemented in this work might be used as a basis to try to understand the complex real relations between shear and turbulence affecting H-mode transport dynamics. They may also pave the path to the development of bidimensional sandpile models that could implement a more realistic view of shear-turbulence interactions.

This project could also help to bring fusion energy research closer to people, helping them to better understand the physical underlying processes and to become less unwilling to fusion when informed about the enormous advantages and potential of fusion over the rest of energy sources.

7. FUSION SOCIO-ECONOMIC FRAMEWORK

7.1 Study of the present and future global energy sector.

The energy revolution is a process taking place this 21st century that has already started at a global scale, due to the increasing global electricity demand and the critical concerns about the current electricity generation methods having harmful effects on the Earth environment. Clean energy is nowadays the most demanded and valued currency seen as the future driver of the global economies [25].

According to this fact, all developed countries are investing and focusing their investigation in the introduction of renewables, the enhancement of the electricity generation capacity and the improvement of the current technologies. Europe is going one step further, acting as an environmentally friendly conglomerate of countries, providing subsidies to the state members for the introduction of the renewables and developing international cooperative projects as ITER with a common objective, save the planet from global warming [26].

The historical evolution and justified forecasts of the global electricity generation for the key years of the renewable energy transition is shown in Figure 7.1, being the second graph a more detailed description of the renewable case (in green colour) shown in the first graph.

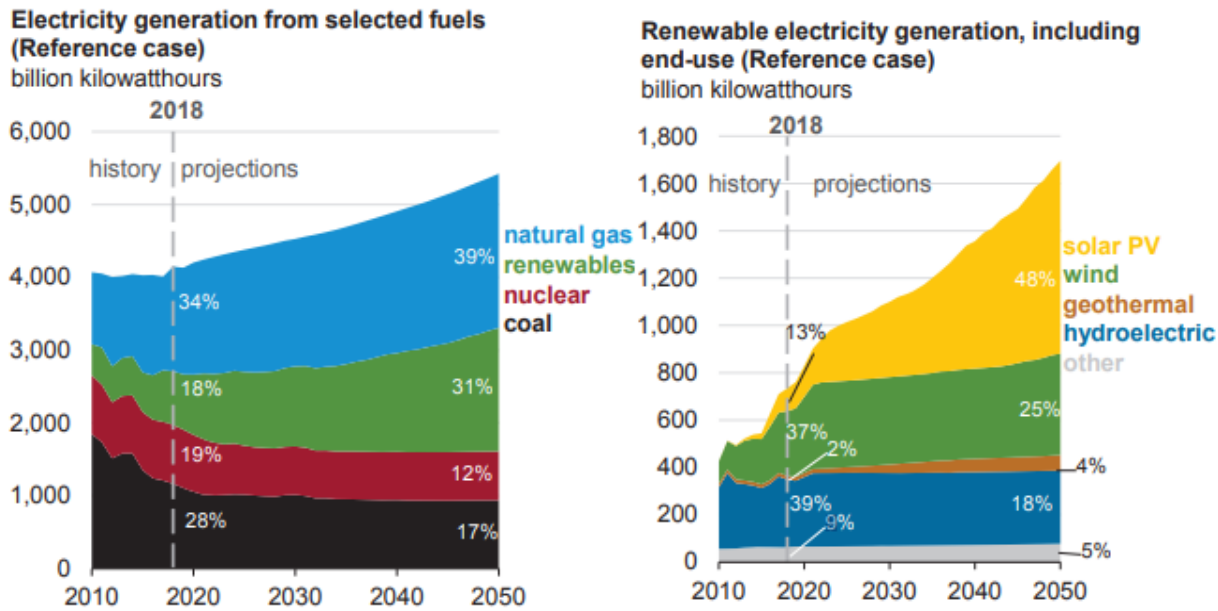

Figure 7.1 Evolution of the global electricity generation methods, with detailed study of the forecast of renewables integration.

The increasing tendency of the different technologies is clearly appreciated specially in case of the solar PV and wind energy, which are proved to have lower CO_2 emissions but higher production costs than the fossil fuels, but what about fusion?

Fusion feasibility is expected to be proved at the first years of ITER operation by the scientific community, increasing the interest of the researchers in performing market studies assuming fusion introduction and making the technology more attractive to private investors. Studies of the expected CO_2 emissions and electricity price of fusion technologies and are shown respectively in Figures 7.2 and 7.3 in comparison with the alternative energy sources.

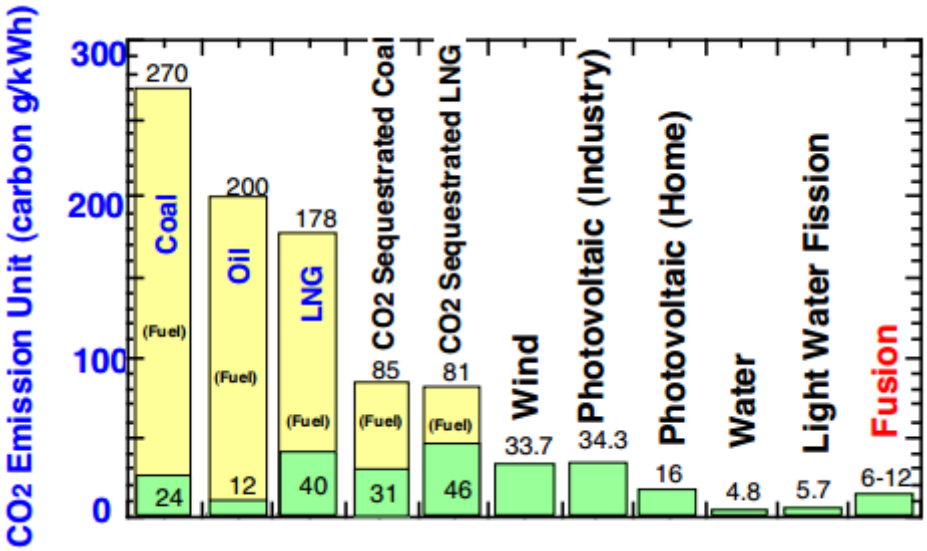

Figure 7.2 CO2 emissions comparison between the future energy sources [Credits to: Ref [27]]

It must be highlighted that Fusion process has been proved to lower the CO_2 emissions [27] in comparison with the most implemented technologies, except the nuclear fission. Providing a potential to improve the current reduction objectives of harmful emissions in electricity production.

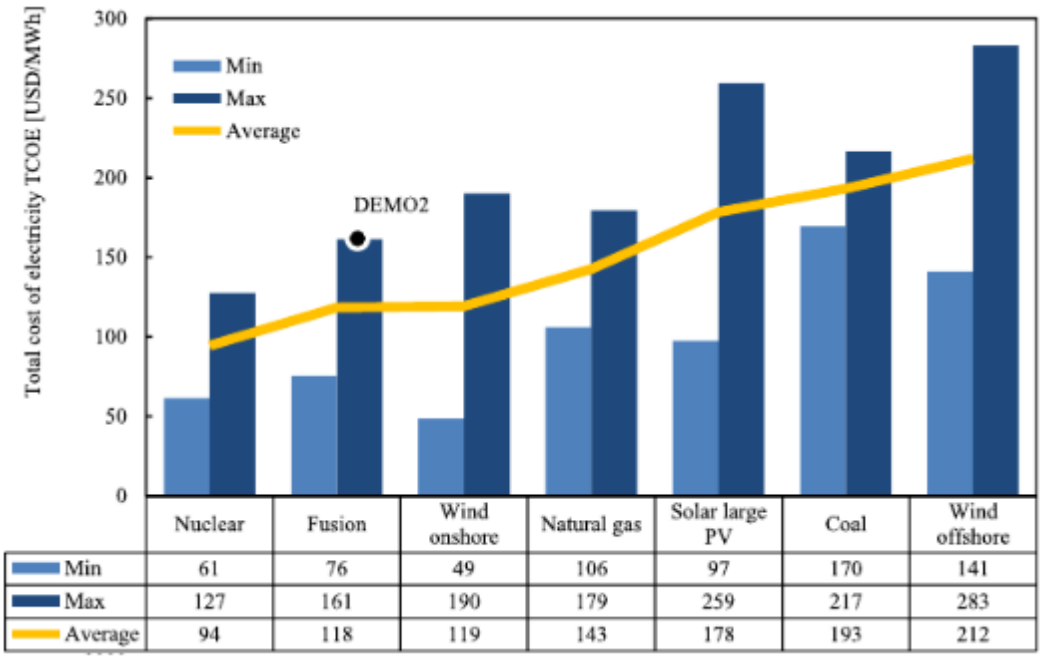

	Nuclear	Fusion	Wind onshore	Natural gas	Solar large PV	Coal	Wind offshore
Min	61	76	49	106	97	170	141
Max	127	161	190	179	259	217	283
Average	94	118	119	143	178	193	212

Figure 7.3 Cost of electricity comparison between the future energy sources [Credits to: Ref. [28]]

Electricity produced by nuclear fusion would also have lower prices than the rest of technologies, being again only outperformed by nuclear fission [28]. Making this technology economically feasible and attractive to enter the market if ITER experiments are found successful.

From the previous analysis actual nuclear fission seems to be a less attractive alternative than fusion energy from an economical point of view. But there are other factors, such as safety and environmental impact. The main features differentiating both technologies are described in the following section.

7.2 Nuclear fusion advantages over fission

- Increased extracted energy:

Nuclear fission is achieved by the splitting of heavy atoms into lighter ones while also realising energy according to Einstein's formula. This is done inside the reactor core by the bombarding of unstable radioactive elements with accelerated neutrons, dividing the nucleus into smaller isotopes and high-speed neutrons, producing several time lower amount of energy than the one produced by fusion, but at starting conditions significantly easier to be reached.

- Lower need of security:

For electricity production to be feasible, the liberated high-speed neutrons from a particular fission reaction are used to bombard the neighbouring nuclei, starting a **chain reaction**. The chain reaction is only monitored when started, since after that moment

the increased number of neutrons produced cause the fission of more and more radioactive atoms at each time, increasing the temperature and complicating the control of the reaction.

The hard stop of the fission is done through strong refrigeration systems and boron control rods that are introduced the reactor to absorb the neutrons. If any of these systems fail, it may lead to catastrophic effects as the explosion of the reactor (for example, Chernobyl, Ukraine) and the release of high levels of radioactivity affecting the area for thousands of years (as in Fukushima, Japan).

On the other hand, in fusion the starting conditions are much more difficult to achieve, and the fusion reaction would immediately stop if not externally maintained. In addition to this, the amount of fuel present inside a fusion reactor is very small (a few grams) and allows the reaction for a few seconds, while many tons of fission fuel are introduced and kept inside the reactor to sustain reactions for several months. In this way fusion reactors would be more easily controlled and intrinsically much safe r than fission reactors.

- Fuel and residues:

The main concern about nuclear fission energy is the disposal of the long-live radioactive fission products and poisonous residues such as plutonium. These have to be buried in radioactive cemeteries which may have harmful effects in the nearby ecosystem.

The only residues coming from a fusion reaction are activated materials (from the reactor walls) with low decaying times that could be reused within 100 years, after proper treatment, again in the reactor.

- Independence from external source:

While the rest of renewable sources depend from an external variable source as the Sun or the wind, the conditions and the driver for fusion energy are manually created, making fusion independent of external conditions and available at all time. If the tritium breeding is also proved feasible, the reactor would be able to self-produce the needed tritium inside the core and would only need the easy extractable lithium from the outside.

7.3 Future of fusion energy

7.3.1 Fusion energy for electricity production

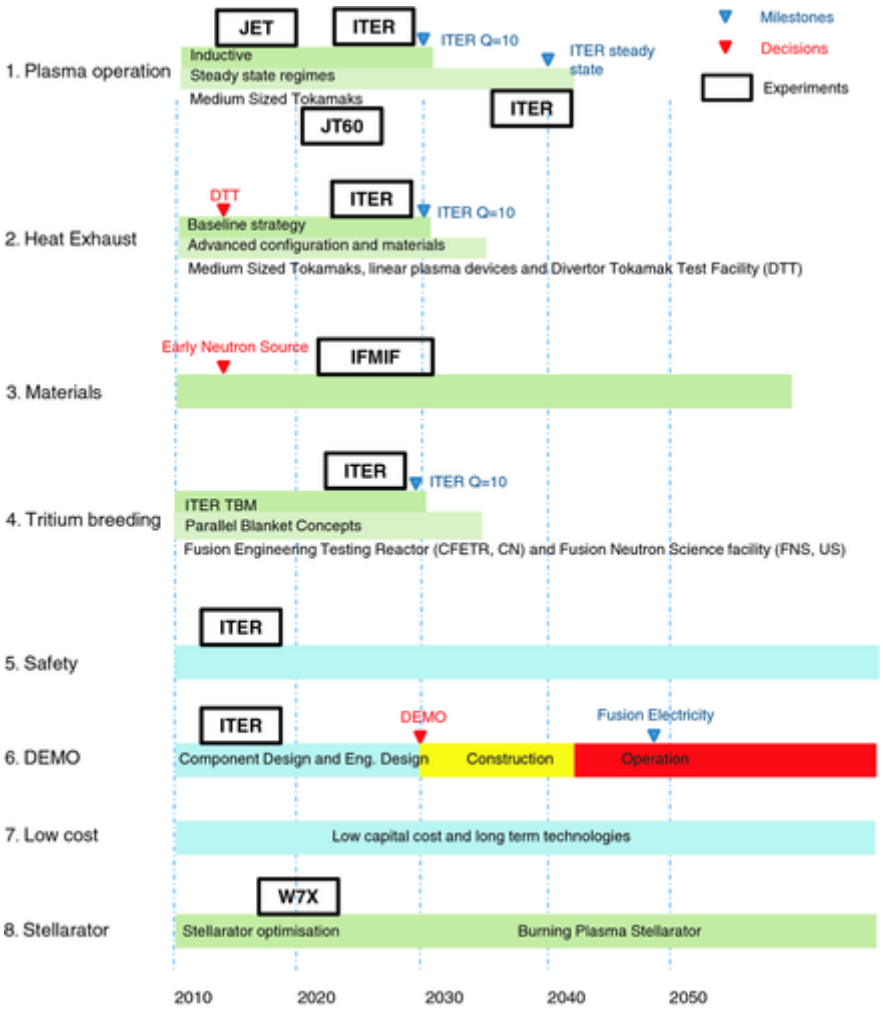

Figure 7.4 Experimental Roadmap for 2010-2050 [Credits to Ref [26]]

Figure 7.4 shows the different experiments that will be performed in the 2010-2050 period in the different experimental reactors to achieve the fusion objectives and have electricity produced by nuclear fusion at the end of the 2040s.

The most important milestone is DEMO, the continuation of ITER experiment if being successful, that would be the first grid connected tokamak fusion reactor of the human history.

7.3.2 Space applications of fusion energy

Independently of current experiments to prove the feasibility for electricity production, nuclear energy and particularly fusion have a huge potential in the development of spacecraft engines. Nuclear reactions are in this context the unique reliable option due to their high energy densities, allowing to reduce the fuel mass whilst providing the same power. In this context, some projects are started to be developed with special importance of the Variable Specific Impulse Magnetoplasma Rocket (VASIMR) engine [29].

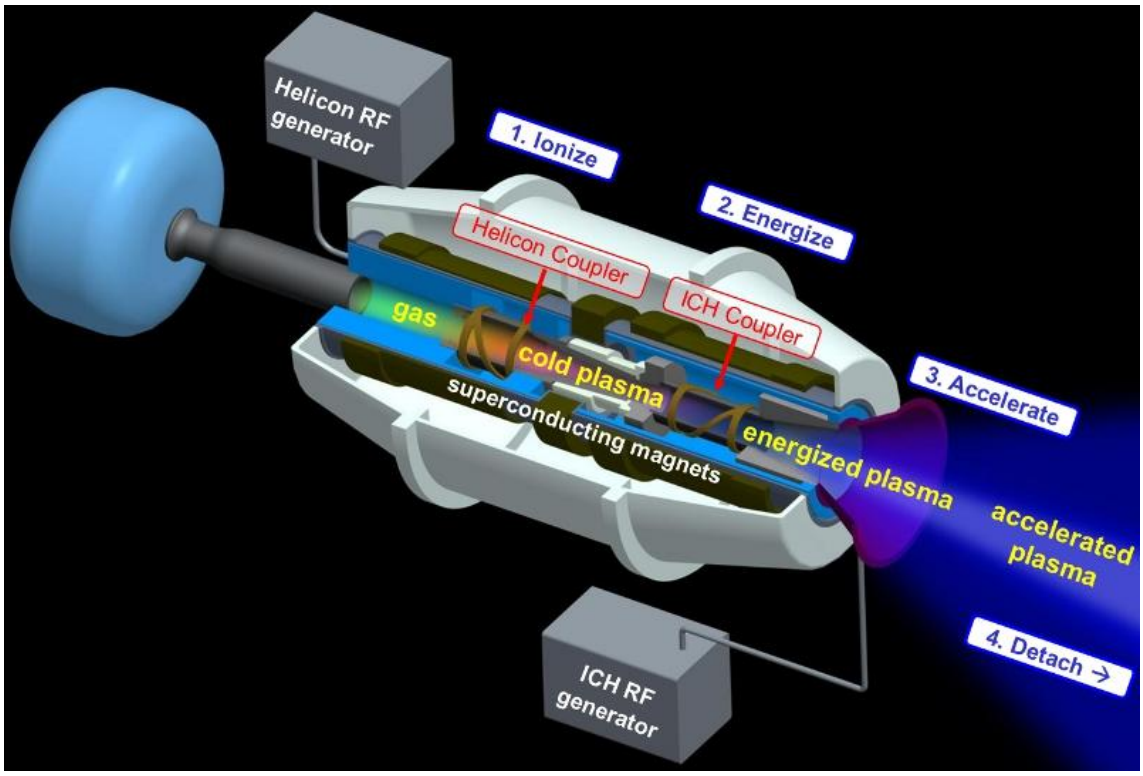

Figure 7.5 VASIMR rocket parts and functioning [Credits to: ADASTRA Company www.adastrarocket.com]

The VASIMR engine is currently being developed by ADASTRA Rocket Company, which consists of an electrical engine that extracts energy from hydrogen plasma. This revolutionary design only needs hydrogen fuel to exit the atmosphere, afterwards hydrogen is collected from the outer space, converted into plasma by ionization in the Helicon RF and then used as propulsion fuel.

Three main characteristics make this concept the most promising design for a future nuclear-electric spacecraft engine, differentiating it from another plasma thruster approaches:

- The capability to optimize its exhaust parameters depending on mission requirements.

- The usage of electromagnetic (RF) waves to generate the plasma, having no physical material electrodes in contact with the hot plasma, therefore increasing reliability, useful life and power densities.

- The processing of large amount of power potentially allowing travels to the outer of the solar system and its high scalability permitting to easy design higher power versions.

7.4 Project budget

The approximated cost for the development of the present project is calculated in the following tables. Costs have been calculated through estimations based on salaries of the main energy companies and the official BOE [30] and are divided in: direct (labour and computer) and indirect costs:

TABLE 7.1. LABOUR COSTS

Worker status	**Time (h)**	**Salary per hour [€/h]**	**Total salary [€]**
Graduate	550	15.75	8662.5
Doctor	80	35.83	2866.4
Total			**11528.9**

TABLE 7.2. COMPUTER COSTS

Tool	**Concept**	**Cost [€]**
Matlab®	Annual license	800
Office 365 Business ®	Annual license	130
Bibliography Access	Access costs	1100
Total		**2030**

Matlab license pricing available at https://es.mathworks.com/campaigns/products
Microsoft office price is foundhttps://products.office.com/

Indirect cost, estimated as a 44% of the direct costs and tax are included in Table 7.3:

TABLE 7.3. TOTAL BUDGET

Concept	**Cost [€]**
Labour costs	11528.9
Software licensing and accesses	2030
Indirect costs (44%)	5985.92
Taxes (21%)	4106.51
Total	**23661.32**

8. REGULATORY FRAMEWORK.

Strictly referring to the final outcome of this project, a model to help to understand the basic dynamics of the plasma inside a tokamak implemented using computer software, there are limited regulations directly applying to this project.

In Spain this matter is regulated by the Código de Propiedad Intelectual [31], which registers the different laws applying to created works.

On the other hand the external context and potential energy market for fusion energy, if proved to be economically feasible, would be strongly regulated in the following years. It would be mainly influenced by the increasing fundamental concerns about the actual harmful methods of producing electricity, specifically for nuclear energy, the greenhouse gases emission and the radioactive waste disposal.

According to this fact the European Commission has developed and implemented a corrective plan called "Energy strategy and energy union". Which defines the energy objectives for years 2020, 2030 to be continued until 2050 and explains the different corrective actions needed to achieve a sustainable unitary model. Including subsidies for investigation and implementation of renewables and regulating penalties in case of lack of fulfilment of the energy objectives [32].

The energy targets are hereby explained:

- 2020: 20% reduction in the greenhouse gases (compared with 1990 values), 20% of renewable energy and 20% energy efficiency improvement.
- 2030: 40% reduction in the greenhouse gases (compared with 1990 values), 32% of renewable energy and 32.5% energy efficiency improvement.

More concretely in the context of fusion energy, the organization in charge of the current regulation and international collaboration and coordination is The International Atomic Energy Agency (IAEA). Some of the international agreements negotiated by the IAEA states member regarding fusion are:

- Integrated Approach to Safety Classification of Mechanical Components for Fusion Applications, IAEA-TECDOC-1851, IAEA, Vienna (2018)

- Investigations of Materials under High Repetition and Intense Fusion Pulses, IAEA-TECDOC-1829, IAEA, Vienna (2017).

- Atomic and Plasma–Material Interaction Data, Atomic and Plasma–Material Interaction Data for Fusion No. 17, IAEA, Vienna (2017).

9. BIBLIOGRAPHY

[1] A. Eddington, *The Nature of the Physical World: Gifford Lectures (1927).* 2012.

[2] A. Einstein, "Ist die Trägheit eines Körpers von seinem Energieinhalt abhängig?" *Annalen Der Physik,* vol. 323, *(13),* pp. 639-641, 1905.

[3] R. Sánchez and D. Newman, "Primer on complex systems," in *A Primer on Complex Systems*Anonymous 2018, .

[4] J. Ongena, "Fusion: A true challenge for an enormous reward," in *EPJ Web of Conferences,* 2015, .

[5] J. D. Lawson, "Some criteria for a power producing thermonuclear reactor," *Proceedings of the Physical Society.Section B,* vol. 70, *(1),* pp. 6, 1957.

[6] J. Lindl, "Development of the indirect-drive approach to inertial confinement fusion and the target physics basis for ignition and gain," *Phys Plasmas,* vol. 2, *(11),* pp. 3933-4024, 1995.

[7] H. Grad, "Toroidal containment of a plasma," *The Physics of Fluids,* vol. 10, *(1),* pp. 137-154, 1967.

[8] M. Wakatani, *Stellarator and Heliotron Devices.* 1998*95*.

[9] J. Wesson and D. J. Campbell, *Tokamaks.* 2011*149*.

[10] J. R. Martın-Solıs *et al*, "Momentum–space structure of relativistic runaway electrons," *Phys Plasmas,* vol. 5, *(6),* pp. 2370-2377, 1998.

[11] G. Becker, "Electron temperature profile invariance on OH, L-and H-mode plasmas and consequences for the anomalous transport," *Nucl Fusion,* vol. 32, *(1),* pp. 81, 1992.

[12] M. Greenwald *et al*, "Transport phenomena in Alcator C-Mod H-modes," *Plasma Phys. Controlled Fusion,* vol. 40, *(5),* pp. 789, 1998.

[13] F. Wagner *et al*, "Development of an edge transport barrier at the H-mode transition of ASDEX," *Phys. Rev. Lett.,* vol. 53, *(15),* pp. 1453, 1984.

[14] R. Sanchez and D. E. Newman, "Self-organized criticality and the dynamics of near-marginal turbulent transport in magnetically confined fusion plasmas," *Plasma Phys. Controlled Fusion,* vol. 57, *(12),* pp. 123002, 2015.

[15] T. Hwa and M. Kardar, "Avalanches, hydrodynamics, and discharge events in models of sandpiles," *Physical Review A,* vol. 45, *(10),* pp. 7002, 1992.

[16] R. Sánchez, D. E. Newman and B. A. Carreras, "Mixed SOC diffusive dynamics as a paradigm for transport in fusion devices," *Nucl Fusion*, vol. 41, *(3)*, pp. 247, 2001.

[17] P. W. Terry, "Suppression of turbulence and transport by sheared flow," *Reviews of Modern Physics*, vol. 72, *(1)*, pp. 109, 2000.

[18] B. A. Carreras *et al*, "A model realization of self-organized criticality for plasma confinement," *Phys Plasmas*, vol. 3, *(8)*, pp. 2903-2911, 1996.

[19] Fukuda Midori Cristina, "Study of Magnetically Confined Plasma Dynamics with Cellular Automata." , University Carlos III of Madrid, 2018.

[20] H. Biglari, P. H. Diamond and P. W. Terry, "Influence of sheared poloidal rotation on edge turbulence," *Physics of Fluids B: Plasma Physics*, vol. 2, *(1)*, pp. 1-4, 1990.

[21] V. Barbu, "Self-organized criticality of cellular automata model; absorbtion in finite- time of supercritical region into the critical one," *Math. Methods Appl. Sci.*, vol. 36, *(13)*, pp. 1726-1733, 2013.

[22] H. E. Hurst, "Long-term storage capacity of reservoirs," *Trans.Amer.Soc.Civil Eng.*, vol. 116, pp. 770-799, 1951.

[23] T. Schreiber, "Measuring information transfer," *Phys. Rev. Lett.*, vol. 85, *(2)*, pp. 461, 2000.

[24] B. P. van Milligen *et al*, "The causal relation between turbulent particle flux and density gradient," *Phys Plasmas*, vol. 23, *(7)*, pp. 072307, 2016.

[25] Energy Information Administration, "Annual Energy Outlook 2019," Jan 24, 2018.

[26] Y. Bréchet and T. Massard, "Will fusion be ready to meet the energy challenge for the 21st century?" *Journal of Physics: Conference Series*, vol. 717, pp. 012002, 2016. Available: http://dx.doi.org/10.1088/1742-6596/717/1/012002. DOI: 10.1088/1742-6596/717/1/012002.

[27] M. Kikuchi and N. Inoue, "Role of fusion energy for the 21 century energy market and development strategy with international thermonuclear experimental reactor," in *Proceedings of the 18th World Energy Congress, Buenos Aires*, 2001, .

[28] S. Entler *et al*, "Approximation of the economy of fusion energy," *Energy*, vol. 152, pp. 489-497, 2018.

[29] F. Chang Díaz *et al*, "The VASIMR engine: Project status and recent accomplishments," in *42nd AIAA Aerospace Sciences Meeting and Exhibit*, 2004, .

[30] BOE, "**BOE n.45**," 2018.

[31] BOE, "Código de Propiedad Intelectual," 2018.

[32] M. da Graça Carvalho, "EU energy and climate change strategy," *Energy,* vol. 40, *(1),* pp. 19-22, 2012.

ANNEX A: MATLAB CODE OF THE SANDPILE MODEL

```
%if the algorithm is starting a new simulation -> set new=1%if it is
continuing a previous run -> set new=0
new=1;
if new==1
%variable declaration in case of a new run
SP=Zc*N:-Zc:ZSP=[SP 0];
Sn=linspace(Smax,Smax,N);
Zn=linspace(0,0,N);
Zc2=Zc;  %solo para el caso en el que Zc2 no se actualiza
Nf2=Nf/(1+f);
end
%definition of the basic parameter of the sandpile model
N=200;
Zc=linspace(200,200,N);
Nf=linspace(5,5,N);
=0.5;
f=10;
Smax=20;
dS=10^(-3);
deltaS=0.1;
Ni=5*10^7;
Activity=linspace(0,0,Ni);
Totalmass=linspace(0,0,Ni);
Pk=linspace(0,0,N);
%% RUN SANDPILE
for t=1:Ni
    unstable=linspace(0,0,N);
    v=randsrc(1,N,[1,0;Po,1-Po]);
    SP(1:N)=SP(1:N)+v; %the external rain adds grains to random cells
of the system
    for i=1:N
        Zn(i)=SP(i)-SP(i+1); %the gradient of the actual profile is
calculated
    if Zn(i)>Zc2(i) %the actual gradient is compared with the critical
one
        unstable(i)=1; %if grater, the particular cell becomes
unstable
    end
    end
    for j=1:N
    if unstable(j)==1
        Sn(j)=Sn(j)+deltaS; %if the cell is unstable, shear is
enhanced by deltaS
        if Sn(j)>Smax %up to a maximum value of Smax
            Sn(j)=Smax;
        end
    else
        Sn(j)=Sn(j)-dS; %if the cell is not unstable, shear is dumped
by dS
        if Sn(j)<0
            Sn(j)=0; %down to a value of 0
        end
    end
    end
    for k=1:N
        if unstable(k)==1%if the cell is unstable
```

```
            Nf2(k)=Nf(k)./(1+f*Sn(k)/Smax);  %the transport of Nf2
changes accordingly with the shear value
            Pk(k)=P1*(1-Sn(k)/Smax)+P2; %the probabily Pk changes
accordingly with the shear value
            w=rand;
            if w<Pk(k) %if probability is favourable
        SP(k)=SP(k)-Nf2(k); %a particular unstable cell losses Nf2
grains
        SP(k+1)=SP(k+1)+Nf2(k); %and transports them to the adcacent
cell to its right
        Activity(t)=Activity(t)+1; %when a cell is unstable, the value
of the activity is increased
            end
        end
    end
end
```